JOURNAL OF GEOPHYSICAL RESEARCH, VOL. 95, NO. D5, PAGES 5731–5748, APRIL 20, 1990

A Regional Scale Model for Ozone in the United States With Subgrid Representation of Urban and Power Plant Plumes

SANFORD SILLMAN,[1] JENNIFER A. LOGAN, AND STEVEN C. WOFSY

Department of Earth and Planetary Sciences and Division of Applied Sciences
Harvard University, Cambridge, Massachusetts

A new approach to modeling regional air chemistry is presented for application to industrialized regions such as the contintental United States. Rural chemistry and transport are simulated using a coarse grid, while chemistry and transport in urban and power plant plumes are represented by detailed subgrid models. Emissions from urban and power plant sources are processed in generalized plumes where chemistry and dilution proceed for 8-12 hours before mixing with air in a large resolution element. A realistic fraction of pollutants reacts under high-NO_x conditions, and NO_x is removed significantly before dispersal. Results from this model are compared with results from grid models that do not distinguish plumes and with observational data defining regional ozone distributions. Grid models with coarse resolution are found to artificially disperse NO_x over rural areas, therefore overestimating rural levels of both NO_x and O_3. Regional net ozone production is too high in coarse grid models, because production of O_3 is more efficient per molecule of NO_x in the low-concentration regime of rural areas than in heavily polluted plumes from major emission sources. Ozone levels simulated by our model are shown to agree with observations in urban plumes and in rural regions. The model reproduces accurately average regional and peak ozone concentrations observed during a 4-day ozone episode. Computational costs for the model are reduced 25- to 100-fold as compared to fine-mesh models.

1. INTRODUCTION

Elevated concentrations of ozone have been observed at both urban and rural locations in the United States and western Europe. Ozone concentrations exceeding 120 parts per billion by volume (ppbv) frequently occur downwind of major cities. Ozone levels exceeding 80 ppbv have been observed over large regions, greater than 1000 km in extent, during stagnation episodes that may persist for as long as 8 days [e.g., *Guicherit and van Dop*, 1977; *Wolff and Lioy*, 1980; *Mukammal et al.*, 1985; *Logan*, 1989]. Analysis of trajectories for these episodes shows that the air mass had passed over major sources of pollutants during the previous 2-3 days [*Mukammal et al.*, 1985; *Evans et al.*, 1983].

High ozone concentrations pose potential risks for damage to human health and to vegetation [*Environmental Protection Agency*, 1986*a*]. Elevated ozone in rural areas is believed responsible for crop losses of 1 to 2 billion dollars annually [*Heck et al.*, 1982] and may contribute also to the damage observed in the forests of western Europe and the eastern United States [*Skarby and Sheldon*, 1984].

Important early studies of the regional ozone problem were presented by *Hov et al.* [1978] and *Isaksen et al.* [1978*a*]. Emissions of photochemical precursors (NO_x and hydrocarbons) are concentrated in metropolitan areas and at power plants, and distributions of precursors are correspondingly inhomogeneous. Previous models for regional photochemistry have attempted to simulate inhomogeneous concentration fields in detail by adopting fine temporal and spatial resolution [*McRae and Seinfeld*, 1983; *Liu et al.*, 1984; *Carmichael et al.*, 1987; *Chang et al.*, 1987; *Lamb*, 1986; *Venkatram and Karamchandani*, 1987]. The Regional Oxidant model for the northeast United States, for example, uses a grid size of 18 km [*Lamb*, 1986], while the Regional Acid Deposition model uses grid spacing of 80 km in order to cover a larger domain [*Chang et al.*, 1987]. Owing to the large number of grid cells and the short time steps needed in these models, enormous computer resources are required.

Fine-resolution models are best for studies of particular episodes over short time scales, but they are not well suited for study of persistent phenomena (more than 3 or 4 days duration) or for simulation of statistical distributions of pollutants over large areas or for long times (cf. Schere, 1988). The statistical distributions of pollutant concentration define the chemical climate of the region. The impact of pollutants on human health or plants may depend on a variety of statistical characteristics, including peak and mean levels, episodic large-scale events, and recurrence times. It is important therefore to understand the factors that regulate the chemical climate over the United States.

Previous work has shown that ozone production is relatively inefficient for the high concentrations of NO_x (> 1 ppbv) found in urban areas and power plant plumes, as compared with concentrations (<1 ppbv) typical of rural areas, when evaluated per unit of NO_x [*Isaksen et al.*, 1978*b*; *Hov and Isaksen*, 1981; *Liu et al.*, 1987]. Since NO_x is lost rapidly in urban plumes [*Isaksen et al.*, 1978*a*, *b*; *Spicer*, 1982], this nonlinearity can have a major influence on model-derived rural ozone levels and on computed net ozone production for a region. As shown below, models with a grid size as small as 80 x 80 km^2 artificially dilute NO_x from major sources; the consequence is excessive production of ozone in rural areas of these models, overestimation of mean concentrations for NO_x and ozone, and distortion of the frequency distributions for NO_x and ozone concentrations.

This paper presents a computationally efficient method for simulating photochemical production of ozone on regional and global scales using subgrid representations of highly polluted areas. The approach is to simulate rigorously the statistical characteristics of concentration fields for photochemical precursors of ozone and thus to represent accurately the net chemistry of areas with high and low concentrations of NO_x. The model uses a

[1] Now at Department of Atmospheric, Oceanic, and Space Sciences, University of Michigan, Ann Arbor.

Paper number 89JD03139.
0148-0227/90/89JD-03139$05.00

grid of 400 x 480 km^2, incorporating generalized subgrid structures to represent urban and power plant plumes within each grid element. Our model is intended primarily for use as a tool to study chemical climate on regional and continental scales, i.e., to help elucidate the factors controlling mean values, seasonal variations, and extrema for ozone concentrations in rural and forested areas of North America. It will be applied also to simulation of ozone distributions during large scale stagnation episodes, particularly those that persist long enough so that identities of individual plumes are irrelevant. It is designed also to help determine the net quantity of ozone, NO_x, and related pollutants transported from industrialized regions to remote parts of the global atmosphere.

We will demonstrate that our model with subgrid plumes (Plumes model) represents regional photochemistry with accuracy similar to that of an Eulerian grid model with resolution as fine as existing data bases for emissions (20x20 km^2). We will show also that the Plumes model predicts ozone concentrations consistent with observations in urban plumes and in rural areas and that the model simulates observations for a large-scale ozone episode. The Plumes model is 25-100 times faster than the comparable 20x20 km^2 model.

First we discuss distributions of emissions of anthropogenic NO_x and hydrocarbons, since the irregular patterns of emissions define the regional modeling problem. Next we present results of Eulerian grid simulations with various resolutions to elucidate errors associated with coarse resolution. The structure of the Plumes model is then presented and results are compared with Eulerian grid simulations and with observed data.

2. Emission Rates of NO_x in the Eastern United States

Emission rates for NO_x and anthropogenic hydrocarbons are given by the National Acid Precipitation Assessment Program (NAPAP) version 5.2 inventory [*Environmental Protection Agency*, 1986*b*] on a 20x20 km^2 grid for the United States and Canada. Figure 1 gives the cumulative distribution function for NO_x emission rates for a representative region (480 x 800 km^2) of the eastern United States. Total emissions are dominated by a small number of locations with high emission rates: grid squares with NO_x emissions greater than 10^{12} molecules cm^{-2} s^{-1} make up only 8% of the total surface area but account for 65% of the regional NO_x source. Most of the major NO_x sources are associated either with large metropolitan areas or with power plants. At the other extreme, NO_x emissions estimated for rural locations are low. The median NO_x emission rate for the region is just $7x10^{10}$ molecules cm^{-2} s^{-1}, corresponding to a probable afternoon NO_x concentration of 0.2 ppbv or less [*Sillman et al.*, 1990]. The chemistry of air downwind of major sources is quite different from the chemistry of air outside the influence of polluted plumes [*Isaksen et al.*, 1978*a*,*b*; *Hov and Isaksen*, 1981]. Models for regional air quality must therefore treat the major NO_x sources and areas downwind separately from the remainder of a region.

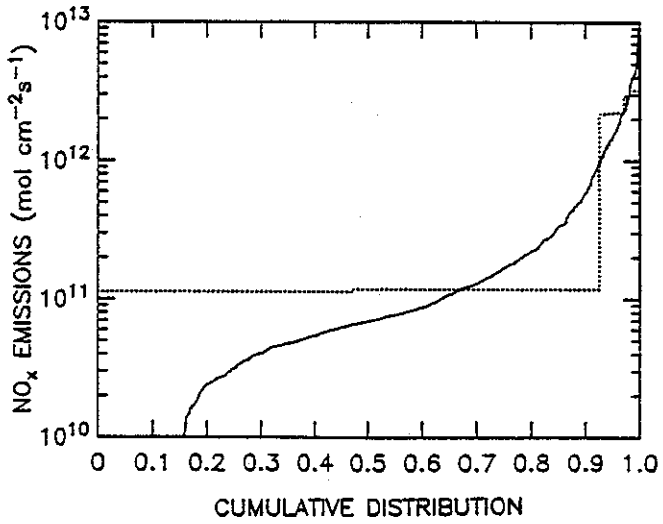

Fig. 1. Cumulative distribution of NO_x emission rates within the 480x800 km^2 region shown in Figure 2, based on the NAPAP version 5.2 inventory for a typical summer weekday. The dotted line shows the distribution of emission rates implicit in the Plumes model formulation, two values each for urban, power plant, and distributed sources.

We define as part of a major NO_x source any 20 x 20 km^2 grid square with emissions exceeding 10^{12} molecules cm^{-2} s^{-1}. This emission rate corresponds approximately to an afternoon NO_x concentration of 4 ppbv, assuming a mixed layer height of 1000 m, a 3 m s^{-1} wind and NO_x concentration of 1 ppbv upwind. The significance of the 4 ppbv cutoff will be discussed below (sections 4 and 5). Urban centers with populations exceeding 100,000, and associated suburban areas, are classified as major NO_x sources according to this criterion. The remaining areas, representing distributed sources, consist of isolated small towns and cities (populations of 50,000 or less) and forested and agricultural areas.

It is useful to divide the major NO_x sources into two categories, one representing predominantly urban sources and the other representing power plants or major industrial sources. Urban areas typically have high emission rates for both NO_x and hydrocarbons, with hydrocarbon to NO_x emission ratios of about 5:1 (carbon atoms:nitrogen atoms) in the NAPAP inventory. Power plant sources are often found in locations with hydrocarbon emissions no greater than the regional average, and associated hydrocarbon to NO_x ratios may be much less than unity. Distinctly different photochemistry characterizes these two regimes. We classify as "urban" all major NO_x sources with a hydrocarbon to NO_x ratio of 1:1 or greater. Major sources with a smaller hydrocarbon to NO_x ratio are classified as "power plants." Our distinction between urban and power plant sources is based on chemistry rather than geography; individual power plants may be included as "urban" sources if anthropogenic sources of hydrocarbons in the same grid box (20x20 km^2) raise the emissions ratio above 1:1. Although somewhat arbitrary, this division provides good separation of first-order chemical differences in plumes from major pollutant sources.

Figure 2 shows the locations of NO_x sources classified as urban or power plant sources by this scheme for typical 480x800 km^2 regions. The correspondence between urban source locations and population centers may be verified by comparing Figure 2 with maps showing the location of cities and towns in the selected regions. The cumulative distribution of NO_x sources with this simplified classification scheme is shown by the dotted line in Figure 1.

Table 1 shows emission rates and total contributions for NO_x and hydrocarbon emissions of urban, power plant and distributed sources for several 400x480 km^2 regions in the United States. Note that regionally averaged NO_x emission rates are rather uniform throughout the eastern United States, but values are lower in the western United States. The relative importance of urban and power plant sources varies greatly from region to region. Note also that, although major sources account for more than half of total emissions, significant quantities of NO_x and hydrocarbons are contributed by distributed sources in almost every region.

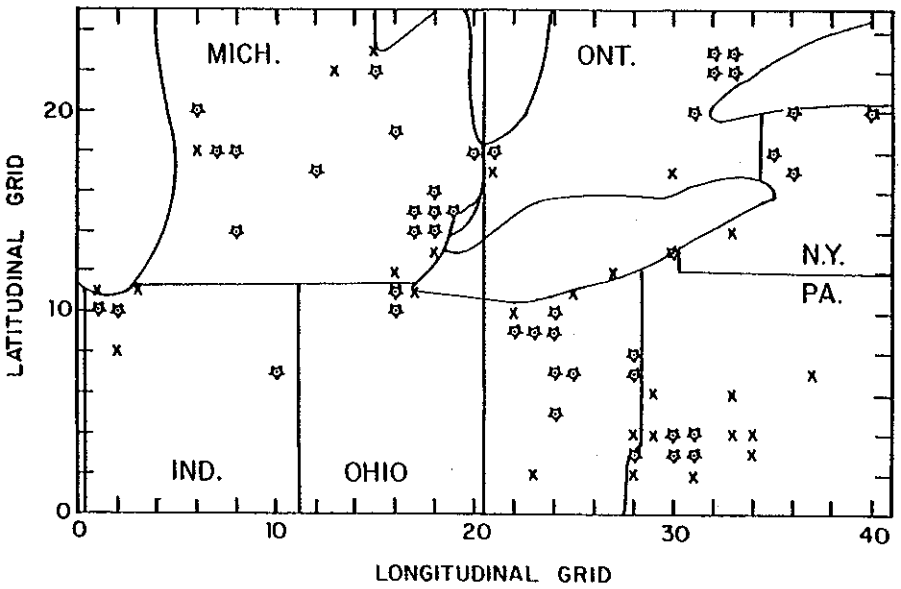

Fig. 2. Location of major NO_x sources within a 480x800 km^2 region of the United States. Points indicate 20x20 km^2 grid squares with emission rates greater than 10^{12} molecules cm^{-2} s^{-1} classified as either urban (stars) or power plant (crosses) sources.

TABLE 1. Regional NO_x and Nonmethane Hydrocarbon (NMHC) Emissions

	Area*, $10^3 km^2$	NO_x, 10^{12} mol. cm^{-2} s^{-1}	NMHC, 10^{12} mol. C cm^{-2} s^{-1}
	Pennsylvania-Ohio region (40°-44°N, 77.5°-82.5°W)		
Regional average	192.0	0.338 (100%)	0.958 (100%)
Urban	10.0	2.220 (34%)	8.25 (46%)
Power plant	6.8	3.22 (34%)	1.34 (5%)
Distributed	175.2	0.118 (32%)	0.527 (49%)
	Michigan region (40°-44°N, 82.5°-87.5°W)		
Regional average	192.0	0.247 (100%)	0.904 (100%)
Urban	7.6	2.18 (33%)	9.08 (36%)
Power plant	3.6	2.94 (22%)	1.13 (2%)
Distributed	180.8	0.113 (45%)	0.556 (61%)
	St. Louis region (36°-40°N, 87.5°-92.5°W)		
Regional average	192.0	0.209 (100%)	0.434 (100%)
Urban	2.8	2.22 (15%)	8.71 (30%)
Power plant	6.8	3.30 (56%)	0.465 (4%)
Distributed	182.4	0.063 (28%)	0.306 (67%)
	Colorado region (37°-41°N, 102.5°-107.5°W)		
Regional average	192.0	0.057 (100%)	0.454 (100%)
Urban	1.6	3.46 (51%)	23.3 (42%)
Power Plant	0.4	1.24 (4%)	0.137 (0%)
Distributed	190.0	0.025 (44%)	0.262 (58%)

NO_x and nonmethane hydrocarbon emission rates are given for both the entire region and for source areas categorized as urban, power plant, and distributed sources within the region for the grid boxes shown in Figure 8.

*Total surface areas of urban, power plant, and distributed source subregions. The numbers in parentheses for NO_x and NMHC give the percentage of total regional emissions originating from urban, power plant, and distributed sources.

3. SIMULATION METHODS

The simulations presented here use the complete chemical mechanism devised by *Lurmann et al.* [1986] with minor modifications introduced by *Jacob and Wofsy* [1988] to extend its applicability to concentrations of NO_x below 1 ppbv. This mechanism provides a detailed treatment of chemistry for a wide variety of anthropogenic hydrocarbons and for the principal biogenic hydrocarbon, isoprene. The mechanism has been tested extensively by comparison with smog chamber experiments and with urban observations [*Lurmann et al.*, 1986; *Sillman*, 1987], and has been used to simulate the chemistry of the boundary layer over the Amazon forest [*Jacob and Wofsy*, 1988]. Half-hour time steps

were used to integrate the differential equations for the mechanism, using an implicit (backward Euler) algorithm.

Photolysis rates were calculated for clear sky conditions at 40°N latitude in July using the Harvard photochemical model [*Logan et al.*, 1981] with updated rate coefficients. Absorption cross sections, quantum yields, and solar flux data were taken from *DeMore et al.* [1985] and a total ozone column of 325 D.U. and surface albedo of 0.15 were adopted. Absorption by aerosols was treated as discussed by *Logan et al.* [1981; Appendix 3]; the aerosol optical depth was 0.68 at 310 nm, based on turbidity data from the eastern United States [*Flowers et al.*, 1969] and the single scattering albedo was 0.75. Photolysis rates were calculated for the midpoint of each model layer.

Emission rates for anthropogenic species were adopted from the NAPAP version 5.2 inventory described above for a typical summer weekday. Emissions of NO_x and anthropogenic hydrocarbons were assumed to vary with time of day according to average diurnal patterns [*Environmental Protection Agency*, 1986*b*]. The daytime average emission rate for isoprene during summer was taken to be 4×10^{11} molecules cms $^{-2}$sec^{-1} [*Lamb et al.*, 1986], varying with time of day to account for solar elevation and for the effect of diurnal temperature variations according to the simple model of *Jacob and Wofsy* [1988].

Uniform species concentrations were assumed for the model domain at the beginning of each simulation, as follows: ozone, 40 ppbv; PAN + other peroxynitrates, 1 ppbv; H_2O_2, 1 ppbv; CO, 250 ppbv; CH_4, 1700 ppbv; hydrocarbons, 15 ppbC; and NO_x, 0.2 ppbv. The water vapor mixing ratio (by volume) was 1.6×10^{-2}. Deposition velocities were assumed as follows: HNO_3, 2.5 cm s^{-1}; O_3 and NO_2, 0.6 cm s^{-1}; NO, 0.1 cm s^{-1}; H_2O_2 and ROOH, 1.0 cm s^{-1}; and PANs, 0.25 cm s^{-1} [*Huebert*, 1983; *Garland and Penkett*, 1976; *Judeikis and Wren*, 1978; *Galbally and Roy*, 1980; *Wesley et al.*, 1982].

We assumed a daily mean surface temperature of 298 K and allowed for temperature variations with time of day and altitude according to

$$T = T_{av} + T_d \sin \omega - HL\,(1 + \sin \omega) \qquad (1)$$

where ω is defined by

$$\omega = 2\pi \frac{\text{hour}-9}{24}$$

T_{av} is the average surface temperature; T_d is the diurnal variation in temperature; H is the altitude of the midpoint of the simulated vertical layer, and L is the lapse rate at 1500. In the simulations below, T_d was taken to be 5 K and L was 8 K km^{-1}. Equation (1) and values for T_d and L are based on data presented by *Trewartha* [1937].

Our simulations with an Eulerian grid model used a simple representation of dynamical transports, designed to provide a framework suitable for studying the effect of horizontal grid resolution on ozone photochemistry. A single vertical layer with a height of 700 or 1500 m was assumed, with a uniform wind blowing throughout the domain. Explicit diffusion was incorporated according to the prescription of *Gifford* [1982], and we minimized the influence of numerical diffusion by adopting winds that followed the orientation of the grid (cardinal directions).

The Plumes model described below adopted the same one-layer structure when it was being compared with Eulerian grid models. Comparisons of the Plumes model with observed ozone concentrations used a more realistic two-layer vertical structure with specified diurnal variation in boundary layer height [*van Ulden and Holtslag*, 1985] as illustrated in Figure 3. The Plumes model is described in section 5, and the two layer treatment of the planetary boundary layer is described in more detail by *Sillman et al.* [1990].

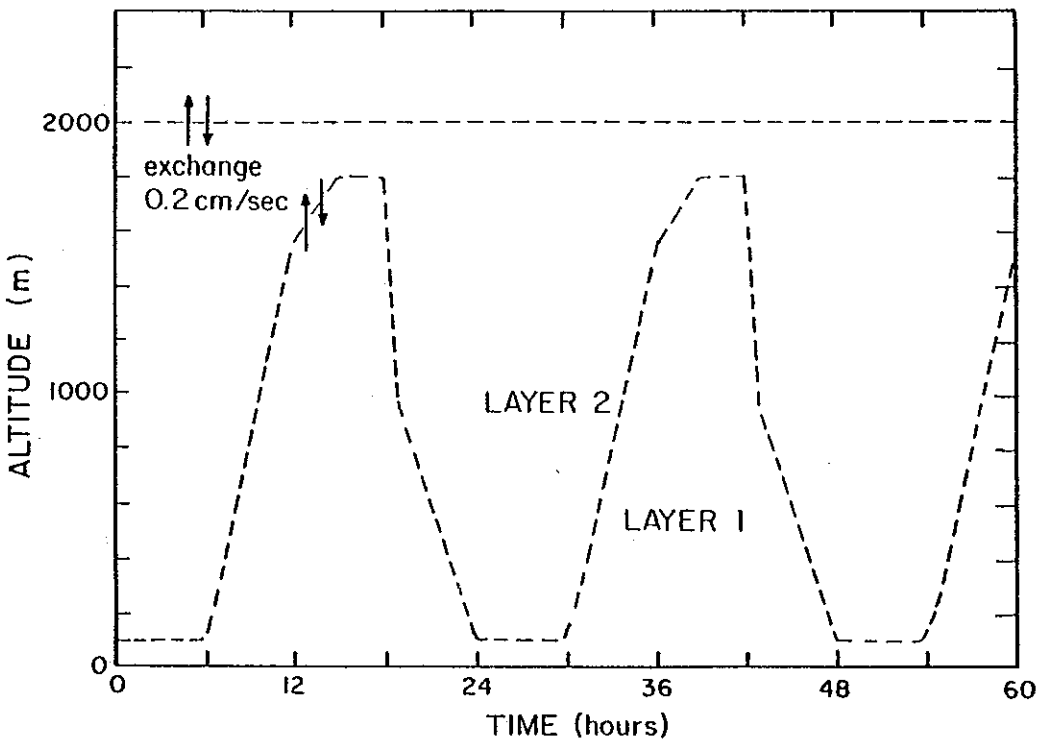

Fig. 3. Diagram of the vertical structure of the two-layer model. The diurnal variation of the mixed layer height is taken from *van Ulden and Holtslag* [1985].

4. EFFECT OF GRID RESOLUTION ON COMPUTED OZONE IN EULERIAN MODELS

In this section we describe simulations of ozone distributions over a region of the northeastern United States (Figure 2) using the simple Eulerian model with various grid resolutions. Our goal is to quantify errors in regional scale models associated with finite grid resolution. This region includes major urban sources and power plants as well as significant portions of the Great Lakes, where emissions are negligible. The simulation discussed in most detail was run for a 20-hour period beginning at 2200 and ending at 1800 the following day, although multiple-day simulations were also run. Winds were assumed easterly at 3 m s^{-1} and the mixed layer height was 700 m, with alternate scenarios considered for comparison. Emission rates for each grid box were computed from the appropriate average of NAPAP emissions.

Figures 4 and 5 show contour diagrams for computed ozone and NO_x concentrations in late afternoon, for models with 20x20 and 80x80 km^2 resolution. High-concentration plumes from major sources are apparent, and the smoothing effect of the 80 km mesh is obvious. Major inland water bodies stand out as low concentration areas in the 20x20 model run but are obscured in the 80x80 run. As might be expected, peak ozone values are higher in the 20x20 run. Less obvious is the important fact that rural ozone levels are higher in the 80x80 run. Similarly, NO_x maxima are higher in the 20x20 than in the 80x80, but low (rural) NO_x values cover larger areas in the 20x20. The effect of smoothing is more drastic for NO_x than for O_3, reflecting the shorter lifetime of NO_x.

Concentrations of OH in the 20 x 20 km^2 model are shown also in Figure 4. Values of OH depend on NO_x in a non linear manner. OH is highest for intermediate values of NO_x, about 2-5 ppbv; OH is lower for high values of NO_x in plumes (e.g., the lower right of the contour plots) and for the low values of NO_x in rural areas. The behavior at low NO_x reflects the role of NO in converting HO_2 to OH; at high NO_x formation of nitric acid acts as an important sink for odd hydrogen at high NO_x. The dependence of OH on NO_x is discussed in more detail by *Logan et al.* [1981] and *Sillman et al.* [1990].

Figure 6 shows cumulative distributions for concentrations of NO_x and O_3 in 20x20 and 80x80 models. The smearing of NO_x from polluted source regions into rural areas in the 80x80 model is readily apparent (note the logarithmic scale used for NO_x). The maximum NO_x concentration is reduced from 44 ppbv in the 20x20 km^2 simulation to 14 ppbv in the 80x80 km^2 simulation. However, NO_x values between the tenth and seventieth percentiles are increased by 10-15% in the 80x80 km^2 run. The increased levels of NO_x in rural areas in the 80x80 km run stimulate excess ozone production and thus lead to artificially elevated ozone levels over more than 85% of the area in the simulation. Ozone in rural areas is higher by 7-10 ppbv in the 80x80 km^2 model than in the 20x20 km^2 model. This behavior reflects greater efficiency for ozone production per unit NO_x at moderate NO_x levels than at high NO_x levels [*Liu et al.*, 1987; *Sillman et al.*, 1990]. The effect is evidently significant in terms of derived air quality for rural areas and for regional net ozone production.

The ozone concentration averaged over the region is shown for various times of day in Figure 7, for simulations with 20x20, 40x40, 80x80 and 400x480 km^2 grid resolutions. Ozone decreases during the night because of deposition and increases during the daytime because of photochemical activity, reaching a maximum in late afternoon. The areas of underestimates and overestimates for ozone (Figure 5) do not balance each other in the regional mean. Regional mean ozone levels for the afternoon increase systematically with coarser resolution. In the run with

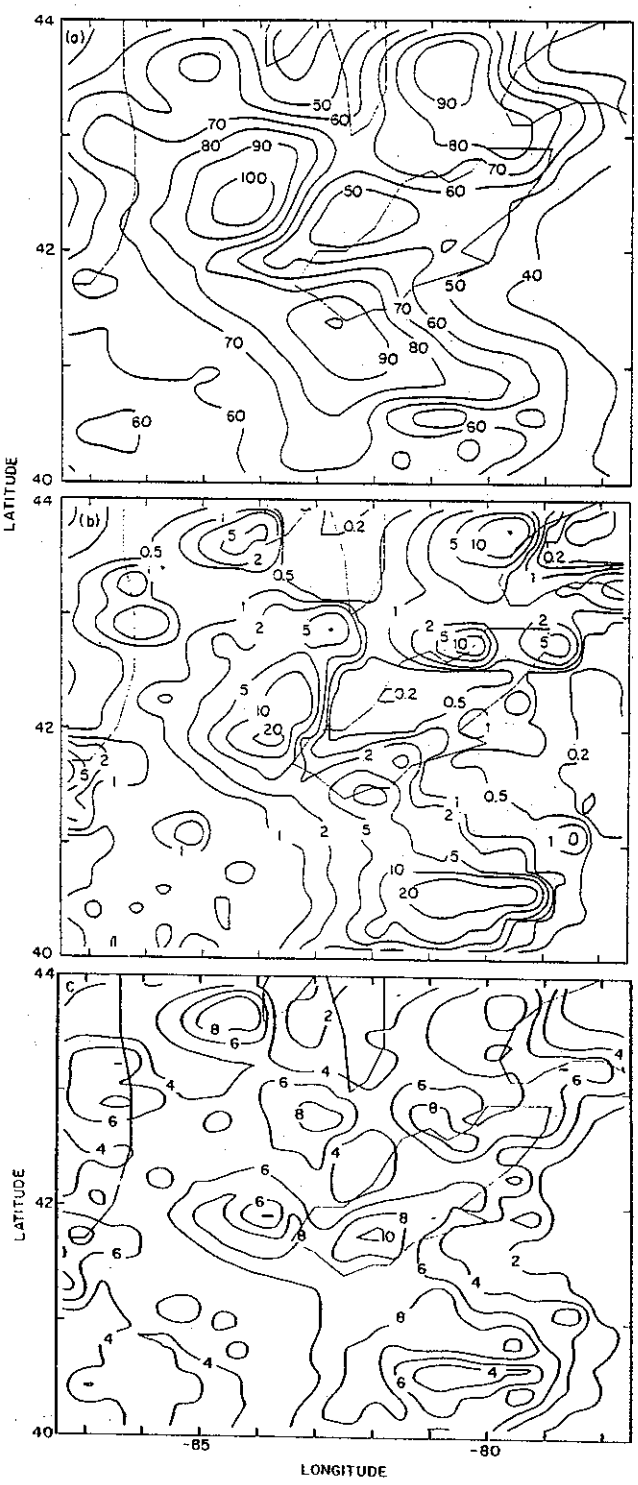

Fig. 4. Spatial variation of (*a*) ozone (ppb), (*b*) NO_x (ppb), and (*c*) OH (10^6 molecules cm^3) at 1400 for the Eulerian model with resolution of 20x20 km^2 for the region shown in Figure 2.

20x20 km^2 resolution, ozone increased from 30 ppbv at 0600 to 63 ppbv at 1800, a net increase of 33 ppbv. This increase was overestimated in the run with 40x40 km^2 resolution by only ~1 ppbv (3%), but the error for the 80x80 km^2 grid was 4.4 ppbv (13%). The run with the 400x480 km^2 grid predicted a net in-

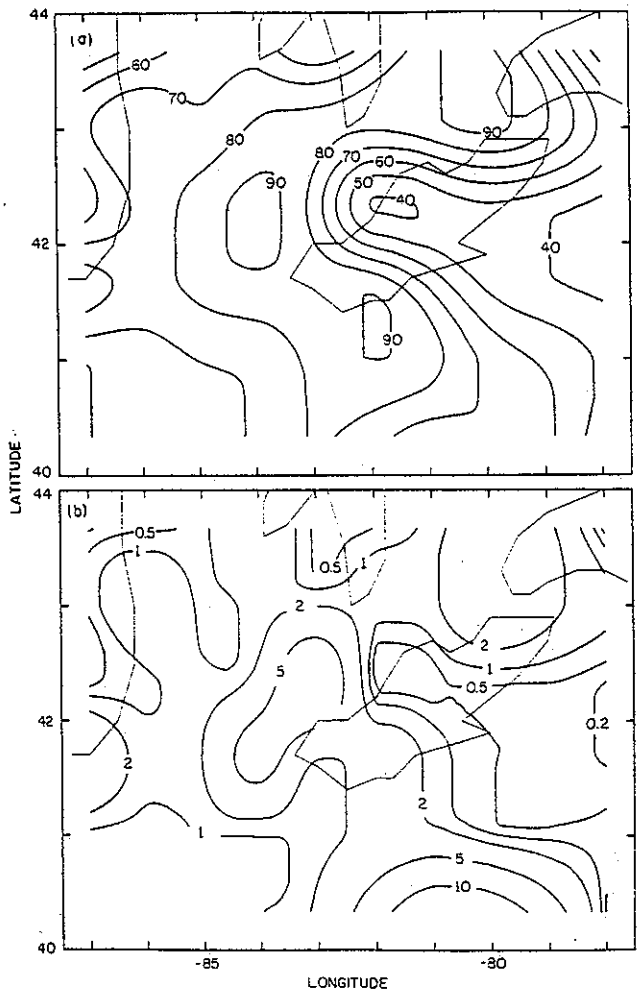

Fig. 5. Spatial variation of (*a*) ozone (ppb) and (*b*) NO_x (ppb) at 1400 for the Eulerian model with resolution 80x80 km^2 for the region shown in Figure 2.

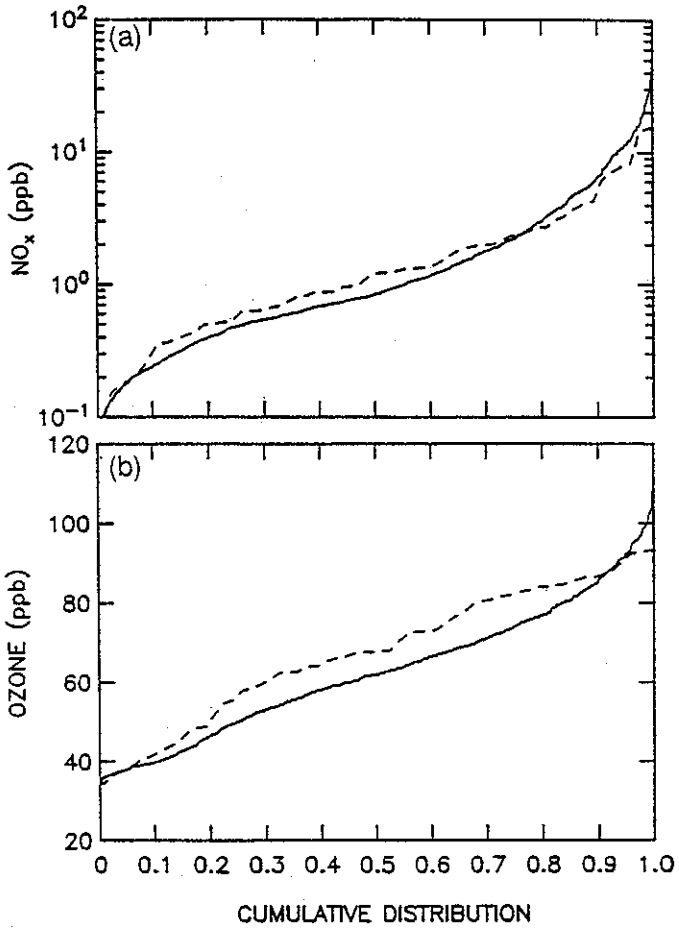

Fig. 6. Cumulative distribution for (*a*) NO_x at 1600 and (*b*) ozone at 1800 in parts per billion for the region shown in Figure 2. Results of the 20x20 km^2 simulation (Figure 4) are shown by the solid line, those for the 80x80 km^2 simulation (Figure 5) by the dashed line.

crease for ozone of 45 ppbv, a 12 ppbv (35%) overestimate. The 400x480 km^2 model overestimated OH and PAN concentrations by similar factors when compared with the 20x20 km^2 simulation. Mean concentrations of NO_x at 1800 were underestimated in the coarse models, but medians were overestimated as expected from Figures 4 and 6.

Eulerian grid simulations were run for several regions in the United States, and a variety of conditions have been assumed for wind speed (3 and 5 m s^{-1}), temperature, boundary layer height, and length of simulation, as shown in Table 2 and Figure 8. The effects of degraded resolution are consistent throughout. Afternoon ozone concentrations in rural areas are overestimated by coarse resolution models, and this effect dominates regional mean values (see Figure 9*a*). Regional average OH is also overestimated in coarse resolution models (Figure 9*b*). Other secondary species (PAN, HNO_3) are similarly overestimated, while reactive primary species (e.g., NO_x) are underestimated in coarse-resolution models.

The tendency for coarse resolution models to overestimate ozone production in rural areas may be explained in terms of the nonlinear dependence of ozone production on NO_x [*Liu et al.*, 1987]. Ozone production becomes inefficient at NO_x levels above about 1 ppbv; photochemical destruction of ozone may occur at high NO_x. These chemical effects reflect the importance of NO_x as a sink for odd hydrogen radicals when NO_x levels are high

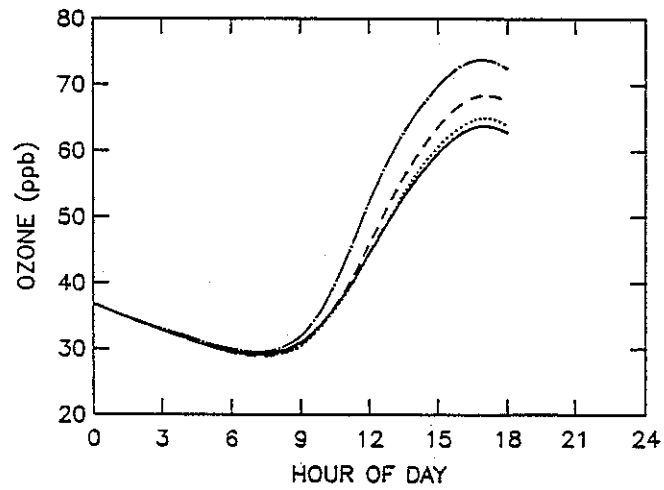

Fig. 7. Regionally averaged ozone (ppb) versus time calculated by the Eulerian model with resolution of 20x20 km^2 (solid line), 40x40 km^2 (dotted line), 80x80 km^2 (dashed line), and 400x480 km^2 (dot-dashed line).

[*Isaksen et al.*, 1978*b*;*Liu et al.*, 1987; *Sillman et al.*, 1990]. Figure 10 illustrates the non-linear relation between ozone and NO_x, based on calculations described in detail elsewhere [*Sillman et al.*, 1990]. Significant overestimates of ozone production are likely

TABLE 2. Description of 11 Test Simulations Used in Evaluation of the Eulerian Grid Model and the Plumes Model

Simulation	Location	Wind Direction and Speed, m s^{-1}	B.L. Height, m	Temperature, K
A	PA, MI	E 3	700	298
B[ab]	NY, PA	W 3	700	298
C[a]	NY	E 3	1500	298
D[a]	PA	S 3	1500	298
E[c]	PA	W 3	700	293
F	PA, MI	W 5	1500	298
G[b]	CI, SL	W 3	1500	298
H[a]	CI	W 3	700	298
I[a]	CI	W 5	1500	298
J[ad]	CI	N 3	700	285
K[ad]	CO	W 3	1500	303

Abbreviated locations refer to 400x480 km^2 grid boxes in Figure 8. Temperature represents diurnal average value with variation with time of day and altitude as indicated in equation (1). All simulations are for a 1-day time period and have an afternoon relative humidity of 50% unless noted otherwise.

[a]Simulation was for a 2-day time period.

[b]Emission rates for anthropogenic hydrocarbons were twice the values given in the NAPAP version 5.2 inventory.

[c]Simulation was for cloudy conditions with 50% attenuation of clear-sky photolysis rates. Temperature remained constant with time and altitude in this simulation. The water vapor mixing ratio (by volume) was 8 x 10^{-3}.

[d]The water vapor mixing ratio (by volume) was 8.0 x 10^{-3}.

when a single grid box contains subregions with both low (<1 ppbv) and high (>3 ppbv) NO_x. The potential for error is greatest when hydrocarbon concentrations are uniformly low (e.g., power plant plumes). The error should be smaller if hydrocarbon concentrations increase in proportion to NO_x, as is typical for urban sources, but significant errors are still likely if NO_x concentrations range over an interval of 4 ppbv or more. Note also that the ozone-NO_x relation is more nearly linear within low-NO_x (0-2 ppbv) and high-NO_x (4-7 ppbv) subdomains; errors due to nonlinear chemistry are most likely for NO_x concentrations between 2 and 5 ppbv. Concentrations of OH and other secondary species are affected by similar nonlinear errors.

5. THE PLUMES MODEL FOR REGIONAL AIR CHEMISTRY

The Plumes model introduced here uses a new approach for including the effects of local emission sources in regional, continental, or global-scale models. Like other photochemical models, the Plumes model operates by dividing the model domain into subcategories and calculating photochemical production and loss terms based on average concentrations of chemical species within each subcategory. In Eulerian models, partitioning is based on a geometric grid, i.e., photochemistry is calculated on the basis of average concentrations within each grid box. In the Plumes model, partitioning into subcategories is based instead on proximity to major emission sources. The Plumes model uses a regional-scale grid (400x480 km^2) along with the following partitioning into subcategories within each grid box: (1) 0 to 4-hour urban plumes (i.e., locations 0-4 hours downwind of urban sources), (2) 4 to 8-hour urban plumes; (3) 8 to 12-hour urban plumes; (4) 0 to 4-hour, 4 to 8-hour, and 8 to 12-hour power plant plumes; and (5) rural (i.e., the remainder of the region).

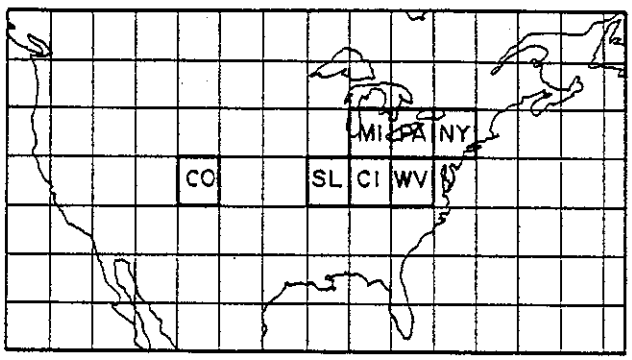

Fig. 8. Locations of 400x480 km^2 grid boxes used in the tests of the Eulerian grid model and the Plumes model. Boundaries correspond to 36°, 40°, and 44°N latitude and 72.5°, 77.5°, 82.5°, etc. west longitude. Abbreviations are based on locations of the grid boxes: New York, Pennsylvania, Michigan, West Virginia, Cincinnati, St. Louis, and Colorado.

This partitioning was chosen in order to represent the variation in NO_x and hydrocarbon concentrations within each region and to minimize errors due to nonlinear chemistry while retaining a simple subgrid structure. Our analysis of chemistry (Figure 10) showed that production of ozone varies linearly with NO_x for NO_x concentrations between 0 and 2 ppbv. The partitioning was designed to insure that under normal conditions daytime NO_x concentrations should not rise above 2 ppbv in locations contained within the rural subgrid. Partitions between 0 to 4-hour, 4 to 8-hour and 8 to 12-hour plumes, and between urban and power plant plumes, were selected to simulate the frequency distributions for NO_x and other pollutants, as well as the covariances between pollutant classes. Note that our apprroach could be extended to include a third or fourth plume (e.g., to distinguish between large and small cities or to include explicit representation of an individual urban center). Results shown below indicate that regional average concentrations are calculated with satisfactory accuracy using only two plumes, a generic "urban" plume and a generic "power plant" plume. Note also that the Plumes model may be applied to either an Eulerian simulation or to a Lagrangian simulation for a moving air mass. We will show below (section 8) that

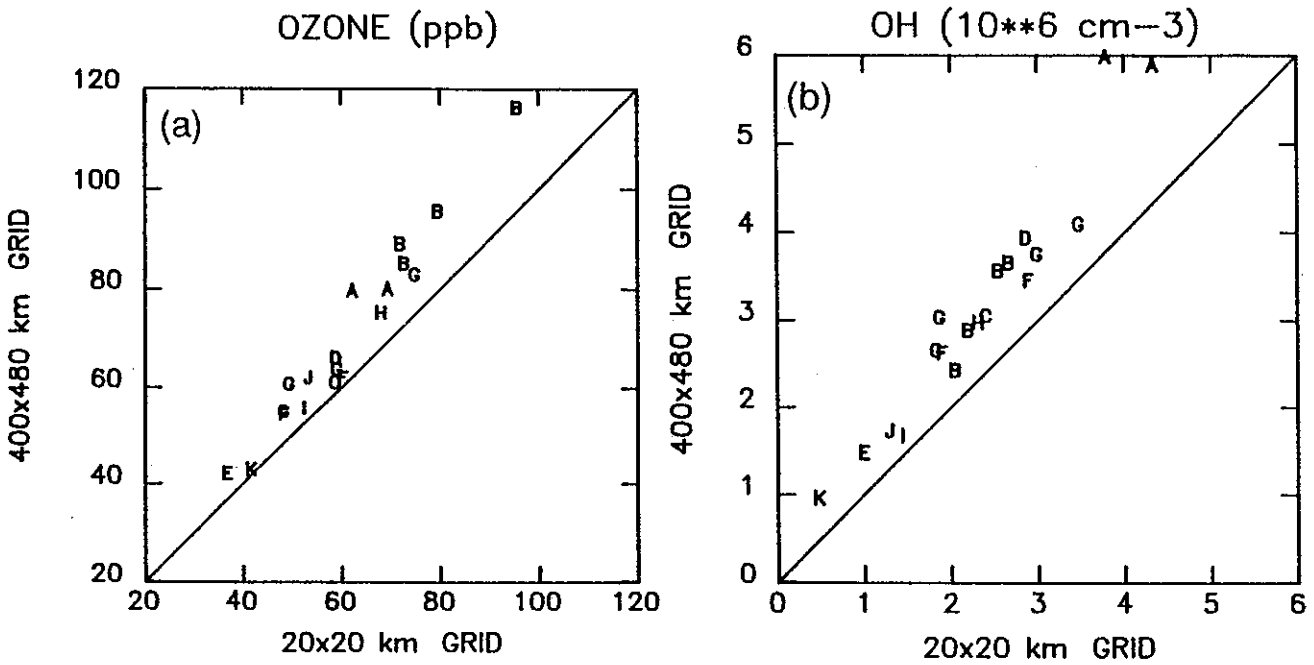

Fig. 9. Average concentration of (*a*) ozone (ppb) and (*b*) OH (10^6 molecules cm^{-3}) at 1600 in each 400x480 km^2 region for the 11 simulations described in Table 2 using a 400x480 km^2 grid (vertical axis) and a 20x20 km^2 grid (horizontal axis). The individual simulations are identified by the letters A-K in Table 2.

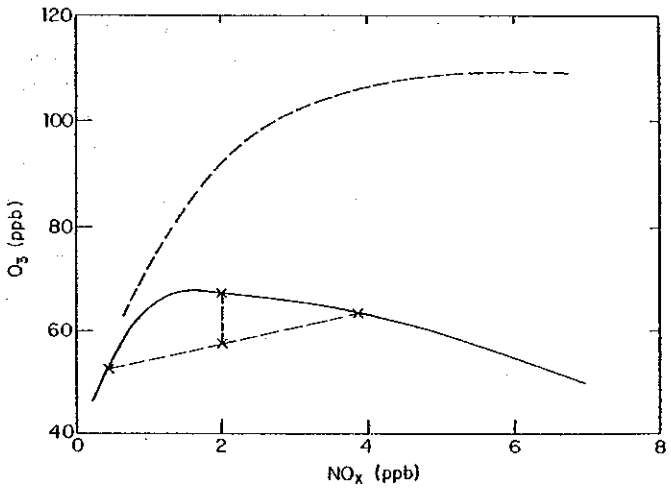

Fig. 10. Calculated values for ozone (ppb) at 1800 as a function of the NO_x concentration at noon for (*a*) 15 ppbC nonmethane hydrocarbons (solid line) and (*b*) nonmethane hydrocarbons increasing in proportion to NO_x (dashed line), based on *Sillman et al.* [1990]. The crosses illustrate a hypothetical calculation of the ozone concentration in a region divided into high-NO_x and low-NO_x subregions. The model using average NO_x (point A') overestimates the ozone averaged for high- and low-NO_x areas (point A).

Eulerian and Lagrangian simulations give similar results for time periods of up to 4 days, assuming a 400x480 km^2 grid.

The following properties of the Plumes model differ from conventional models:

1. The size of each subgrid is not constant. The area occupied by plumes varies with wind speed.
2. Because the partitioning into subgrids is not fixed geographically, the Plumes model predicts the distribution of concentrations within each grid box, rather than concentrations at specific locations.

The Plumes model operates as follows (see Figure 11). At the beginning of every 4-hour time period a new 0 to 4-hour plume is initiated with air drawn from the rural subgrid box. The chemistry in this box is simulated for 4 hours with emissions as defined below. At the end of each 4-hour period air from the 0 to 4-hour box is advanced to the 4 to 8-hour box. The plume is diluted as it enters the 4 to 8-hour box, to account for plume widening (see below). The chemistry in the 4 to 8-hour box is allowed to evolve for a 4-hour period, after which its contents are advanced to the 8 to 12-hour box, diluted with air from the rural box, and allowed to react for an additional 4 hours. At the end of each 4-hour time period the contents of the 8-12 hour box are mixed into the rural box. The 12-hour old plumes typically have NO_x concentrations reduced to 2 ppbv or less as a result of dilution, deposition, and photochemical reactions.

Photochemistry is calculated every 1/2 hour within each plume box. Hence, simulated concentrations in 0 to 4-, 4 to 8- and 8 to 12-hour plumes represent a downwind progression of an evolving urban plume, rather than the average concentration within the subgrid. Only the dilution with rural air is treated discretely at 4 and 8 hours. The choice to simulate downwind progression of plumes ensures a more accurate representation of the variation in NO_x concentrations within each region.

Emission rates in each subgrid box are based on the division of sources within each grid box into urban, power plant, and distributed categories as described above in section 2. Total urban and power plant emissions are entered in the 0 to 4-hour urban and power plant subgrid boxes respectively. Distributed emissions are partitioned among rural, urban and power plant subgrid boxes in proportion to their sizes. Release of emissions within each subgrid is spaced evenly over each 4-hour time period, with a factor representing time-of-day variations. The 0 to 4-hour power plant subgrid box is treated differently because these are most often iso-

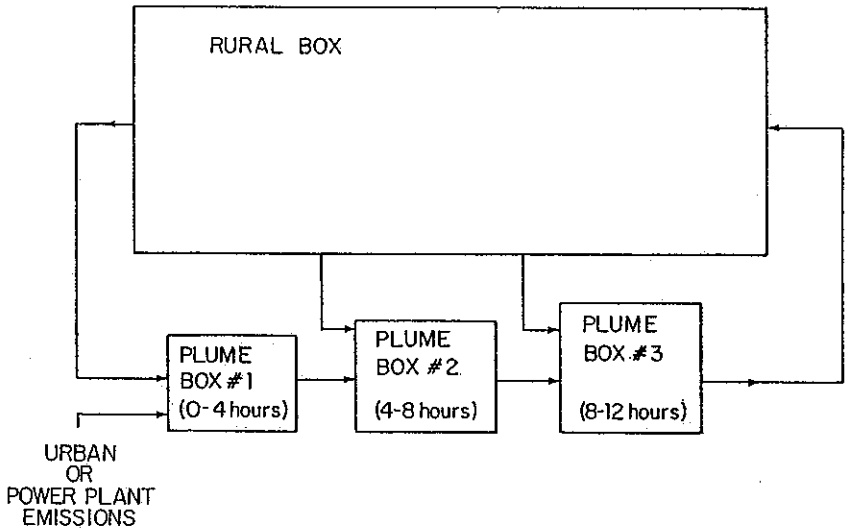

Fig. 11. Diagram of the Plumes model.

lated sources surrounded by rural areas. The bulk of the 'power plant' emissions are introduced in the first half hour of simulation, with the emission rate for the remaining 3.5 hours equal to the rural emission rate.

The area represented by each plume box depends on the number of urban and power plant sources within the region, the wind speed, and the value adopted for the average width of individual source clusters. The generic source width (y) is used to distinguish the behavior of large urban centers or clusters of power plants from that of isolated small cities or power plants. In a large urban center, emissions from several adjacent 20x20 km^2 grid boxes overlap to form a single plume. The difference between a plume generated by adjacent 20x20 km^2 grid boxes and plumes generated by isolated 20x20 km^2 sources is illustrated in Figure 12. Note that the total area occupied by the four isolated plumes is twice the area occupied by the plume from four adjacent sources. Concentrations of primary pollutants are therefore lower for isolated plumes than in plumes from adjacent sources.

The area of the 0 to 4-hour plume box ($A_{0\text{-}4}$) is equal to the area occupied by urban or power plant sources within the 400x480 km^2 region (A_E) multiplied by a factor that accounts for the wind speed and the overlap between adjacent sources, with the constraint that the box area is never smaller than the total source area:

$$A_{0\text{-}4} = \max\left(A_E \frac{W t}{y}\ ;\ A_E\right) \tag{2}$$

where W is wind speed, t is the time interval (i.e., 4 hours) and y is the assumed individual source width. At the end of each 4-hour period a quantity of air is advanced from the 0 to 4-hour box to the 4 to 8-hour box; the remaining contents of the 0 to 4-hour box are diluted with air entering from the rural grid. The area of the advanced portion is

$$A_{adv} = A_E \frac{W t}{y} \tag{3}$$

i.e., the advanced portion represents plume export over a 4-hour period. When winds are light, the 0 to 4-hour box functions as a urban box model, but at high winds the 0 to 4-hour box functions along with the other plume boxes as a Lagrangian model for an evolving plume. The entire contents of the 4 to 8-hour plume box are advanced to the 8 to 12-hour plume box at each 4-hour interval regardless of wind speed. The areas occupied by the 4 to 8-hour and 8 to 12-hour plume boxes are equal to areas advanced from the prior 0 to 4-hour and 4 to 8-hour boxes multiplied by a factor that represents plume spreading and associated dilution. The dilution factor is calculated from the width of the representative source using the Gaussian solution to the Fickian diffusion equation [*Csanady*, 1973]

$$\frac{d\sigma}{dt} = \frac{K_D}{\sigma} \tag{4}$$

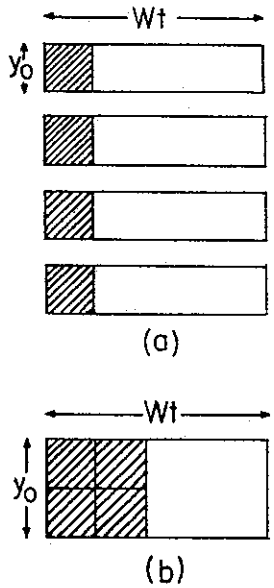

Fig. 12. The effect of plume width on species concentration within the plume. The four individual sources in Figure 12*a* and the single source in Figure 12*b* have the same area and total emissions. However, the four plumes in Figure 12*a* occupy an area twice as large as that from Figure 12*b*, and hence pollutant concentrations are larger in Figure 12*b*. The dependence of the plume area on plume width (y), wind speed (W) and the length of the time step (t) is given by equation (2). A generic plume as in Figure 12*a* would be appropriate for a region with many small sources, while the representation in Figure 12*b* would be appropriate for a region with one or more large metropolitan areas.

The plume width y_t is equal to twice the Gaussian variance (σ) and is obtained by integrating equation (4):

$$y_t = [\, y_0^2 + 8K_D t \,]^{1/2} \quad (5)$$

The diffusion coefficient, 10^4 $m^2 s^{-1}$, was taken from analysis of observations [*Gifford*, 1982].

The area occupied by the rural box is equal to the area remaining within the region after accounting for the plume boxes. Average species concentrations within the region are found by taking a weighted average of concentrations in each subgrid box. Area-weighted distribution functions for pollutant concentrations are computed from areas and concentrations of the various subgrid elements.

A width was adopted for the generic urban source in each region by dividing the total emission rate for NO_x (in molecules per second) for the largest metropolitan area by the mean emission flux (in molecules per square centimeter per second) for all urban sources in the region and taking the square root. Total emissions for the representative urban source thus match total emissions from the major metropolitan center in the region, but the emission flux (per unit area and time) is characteristic of the mean for all urban areas in the region. This approach allows realistic simulation of areas associated with urban plumes and of concentrations of pollutants in the dominant urban plumes for most regions of the eastern United States. The value selected for the urban width, if approximately realistic, has little effect on rural ozone (see section 7), but it can have a larger effect on peak concentrations predicted within the plume. Some typical urban widths in the Plumes model are 80 km for New York, 60 km for Detroit, and 45 km for St. Louis.

The width for power plant sources was established by calculating the average of the effective widths of all power plant clusters in the region, weighted by NO_x emissions from the cluster. We defined a "cluster" of power plant sources as a group of individual sources separated by no more than 20 km. Effective width is equal to the square root of the area occupied by sources making up a cluster, for example, a cluster comprising four 20x20 km^2 sources has an effective width of 40 km. With this method a width of 30 km was selected for power plants in the Pennsylvania grid box, and widths ranging from 20 (the smallest size possible based on the NAPAP inventory) to 24 km were selected for power plants in other grid boxes.

Advection from one 400x480 km^2 region to another requires special treatment in the Plumes model because the air advected between regions is itself partitioned into rural, urban and power plant plume subgrids. The total plume volume that crosses grid boundaries may be calculated using a standard advection scheme, given assumptions concerning the location of the major plumes in the grid box; in practice, we account for the location of plumes within the grid box using a moments scheme as discussed below. Similarly, the total air mass transfer between grid boxes may be calculated using standard schemes. In order to conserve mass, the volume of advected rural air must be found by subtracting the advected plume volume from the total intergrid advection. Having determined the size and partitioning of the advected air mass, we calculate the contents and partitioning of the 400x480 km^2 grid boxes by combining the residual and advected subgrids (i.e., residual and advected rural subgrids, 8 to 12-hour urban plumes, etc.).

In three-dimensional models a moments scheme [e.g., *Prather*, 1986] may be used to account for gradients of individual species within grid boxes. The moments scheme allows any spatially varying function $f(x,y)$ to be approximated by a second-order polynomial with coefficients equal to zero-, first-, and second-order moments. The modified distribution of $f(x,y)$ due to advection is calculated based on these moments. In the Plumes model we have used moments to represent the spatial distribution of the volume of air and masses of individual species within each subgrid. Volume moments for the 0 to 4-hour plume subgrids are determined from the locations of plume sources, and are derived from equation (2) and the vertical layer thickness. Moments for individual species are then computed by multiplying the volume moments by the calculated species concentrations. Moments for 4 to 8-hour and 8 to 12-hour plume subgrids are found by calculating 4-hour advection of moments for the prior subgrid (0 to 4-hour and 4 to 8-hour plumes). Moments for the rural subgrid are updated at each time step to account for transfers of air to and from the various plume subgrids in accordance with linear superposition.

6. COMPARISON BETWEEN RESULTS FROM THE PLUMES MODEL AND A 20x20 km^2 GRID MODEL

Figure 13 shows a comparison between average ozone concentrations calculated by the Plumes model and concentrations calculated by the Eulerian grid model for the simulations described in detail in section 4. Results are shown for two versions of the Plumes model: one in which plumes are followed for a total of 12 hours before mixing into the rural box, and a second version in which plumes are followed for 8 hours. The latter version reduces the number of boxes required for each 400x480 km^2 region by 30%, from seven to five.

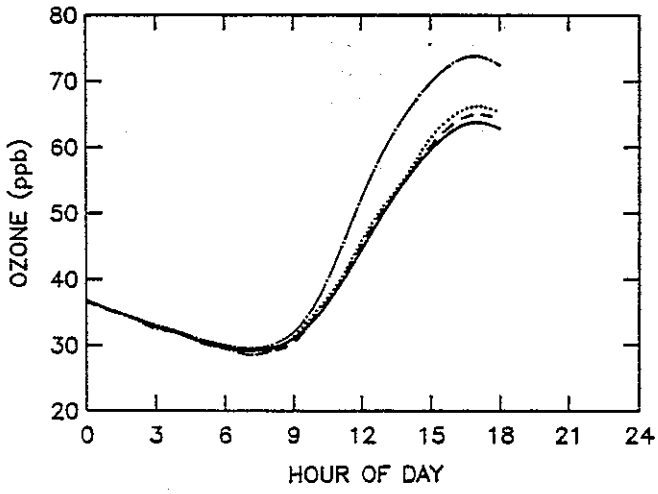

Fig. 13. Ozone (ppb) versus time in the Plumes model simulations with (*a*) plumes followed for 12 hours (dashed line) and (*b*) plumes followed for 8 hours (dotted line). Results of the Eulerian grid simulation with 20x20 km^2 grid resolution (solid line) and 400x480 km^2 grid resolution (dot-dashed line) are shown for comparison.

Results in Figure 13 show that both versions of the Plumes model almost eliminate the tendency to overestimate ozone that was found in the coarse resolution Eulerian grid models. In the 12-hour Plumes model the net increase in ozone is overestimated by 4% when compared with the 20x20 km^2 Eulerian grid model, as opposed to the 35% overestimate found in the original 400x480 km^2 model. Calculated PAN and HNO_3 concentrations in the Plumes model also agree with the 20x20 km^2 simulation to within a few percent. The NO_x concentration is overestimated slightly (7%). The 12-hour Plumes model is therefore similar in accuracy to the 40x40 km^2 Eulerian model. When the Plumes model is ab-

breviated to follow plumes for 8 hours instead of 12 hours, errors are increased slightly. The error in the net increase in ozone changes from 4% to 7% when compared with the 20x20 km^2 simulation. This result is still considerably better than the 80x80 km^2 Eulerian model.

The dramatic improvement offered by the Plumes model is a consequence of the model's simulation of areas with high and low NO_x (and high and low hydrocarbons and ozone) within the region. The areal distribution of ozone and NO_x in the Plumes model is determined from the concentration in each subgrid box and the associated area (equations (2) and (3) above)). Comparisons between cumulative distributions of ozone and NO_x calculated by the 20x20 km^2 Eulerian grid model and by the Plumes model are shown in Figure 14. The Plumes model reproduces most of the important features of the Eulerian grid distributions. In the Eulerian simulation about 60% of the simulated region has low (< 1 ppbv) NO_x and moderate (40-60 ppbv) ozone concentrations. These conditions correspond closely with conditions in the rural subgrid boxes of the Plumes model. The Eulerian simulation also predicts the occurrence of ozone concentrations of 80-110 ppbv and NO_x concentrations of 10-40 ppbv within the region. These peak concentrations and their spatial extent correspond well to concentrations in, and spatial extent of, the various plume subboxes in the Plumes model. Covariances between different pollutant classes are simulated well.

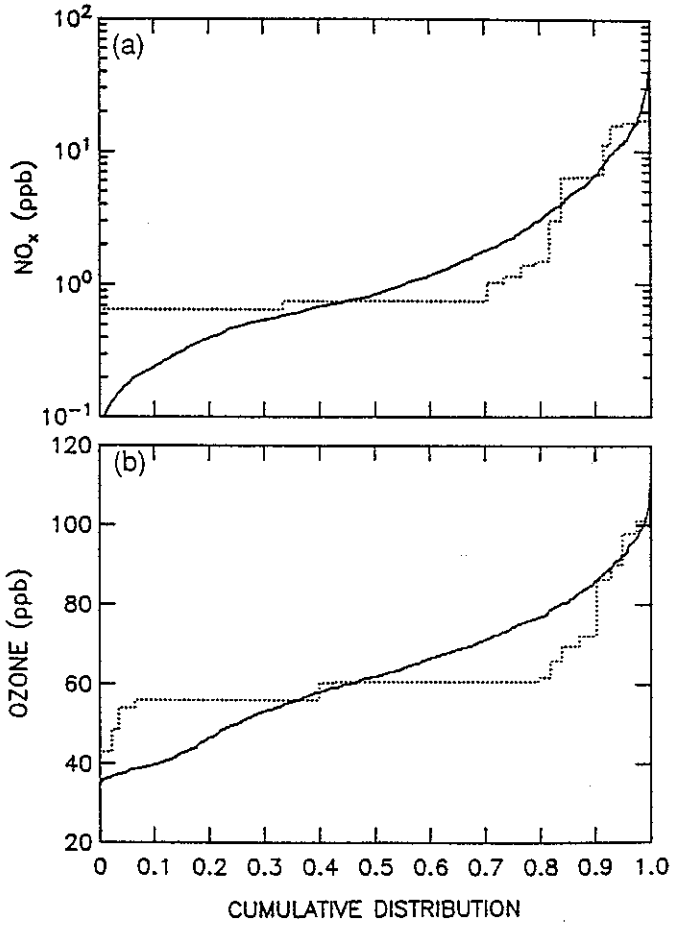

Fig. 14. (*a*) Cumulative distribution for NO_x (ppb) at 1400 within the region shown in Figure 2 calculated by the 20x20 km^2 Eulerian grid model (solid line) and by the Plumes model (dotted line). (*b*) Results for ozone (ppb) at 1800.

The ability to represent accurately the areal distributions of ozone and NO_x within a region is a major advantage of the Plumes model and the inherent reason for its accuracy. We have shown above that errors occur in coarse resolution simulations in large part because they fail to distinguish between subregions of low and high NO_x. The Plumes Model is able to approximate the distribution of NO_x within each region, and hence errors associated with coarse grid resolution are largely avoided.

Another comparison of the Plumes model and the 20 x 20 km^2 Eulerian model is given in Table 3, which shows the budget of NO_x in each. The fate of NO_x is similar in the two models, with conversion to HNO_3 providing the major sink. Dry deposition is a minor sink in each case. Table 4 gives the lifetimes of NO_x in each of the models. The lifetimes become shorter as the plumes become more dilute, and they are shortest in the rural box. Conversion of NO_x to nitrates and PANs becomes more important in the rural box because the higher hydrocarbon to NO_x ratio favors formation of these compounds. Table 5 gives the fate of the NO_x emitted into the urban and power plant plume sub-grids. Only a small fraction of the NO_x, less than 10%, is exported to the rural box.

We have made comparisons between results of the 8-hour Plumes model and the 20x20 km^2 Eulerian model for a wide variety of assumed meteorological conditions and for several regions throughout the northeastern and midwestern United States and for one western region (see Figure 8 and Table 2). Tests of the Plumes model for these simulations duplicate the level of accuracy shown in Figures 13 and 14. We included runs in which hydrocarbon emissions in the NAPAP inventory were doubled. Comparisons between average 1600 concentrations of ozone, PANs, NO_x, and HNO_3 in the Plumes model and in 20x20 km Eulerian simulations are shown in Figure 15. Also shown in Figure 15 are results for the ninety-eighth percentile values of ozone, and for the standard deviation of NO_x concentrations. The Plumes model results for average concentrations compare well with the 20x20 km^2 Eulerian simulation with just a slight tendency to overestimate ozone concentrations, as expected from the discussion of Figures 4, 5, and 14. Peak ozone concentrations in the Plumes model are 10-20% lower than peak ozone in the 20x20 km^2 Eulerian simulation, but there is good agreement for ozone concentrations at the ninety-eighth percentile.

We conclude that the Plumes model achieves an accuracy in simulating regional scale processes comparable to that of a 40x40 km^2 Eulerian grid simulation and within a few percent of that of a 20x20 km^2 model. The time for computation is reduced by a factor of 25 relative to a 40x40 km^2 model and by a factor of 100 relative to a 20x20 km^2 model. This allows use of a complete chemical mechanism in a large-scale simulation, an important step in developing an accurate regional oxidant model [cf. *Schere*, 1988].

7. SENSITIVITY TO MODEL PARAMETERS

We investigated the sensitivity of Plumes model results to values adopted for model parameters. The model allows for interaction between plumes from contiguous urban areas, with the time scale determined by the wind speed and the urban width parameter. However, exchange of pollutants between adjacent urban areas may vary with wind speed or direction. We examined the sensitivity of model results to assumed urban width as a way to examine the adequency of our simple treatment. Table 6 shows regional average concentrations of ozone, OH, and nitrogen species for a range of values. As the width increases, concentrations of primary pollutants within the plume increase (see Figure 12) while those of secondary pollutants decrease. Unless the

TABLE 3. Comparison of NO_x Budget in the Eulerian and the Plumes Models

	Initial Concentration+Import	Emissions	Conversion To HNO_3	Conversion To RNO_3	Conversion To PANs	Dry Deposition	Export	Final Concentration
20x20 km^2	0.10	3.10	1.17	0.33	0.47	0.31	0.11	0.77
Plumes	0.10	3.10	1.15	0.33	0.48	0.28	0.10	0.79
400x480 km^2	0.10	3.10	1.21	0.36	0.64	0.24	0.09	0.53

Values are the cumulative totals of the NO_x sources and sinks for the 20-hour simulation in Figure 13, expressed in 10^{11} molecules cm^{-3} for the entire model domain (480 km x 800 km x 700 m) (10^{11} molecules cm^{-3} ≈4 ppb).

TABLE 4. Lifetime of NO_x (hours)

	HNO_3	RNO_3	PANs	Chemical Loss	Deposition	All Losses
			Day + Night			
20x20 km^2	9.3	32.7	22.3	5.5	38.1	4.8
Plumes Model	10.1	34.9	25.2	6.0	38.2	5.2
400x480 km^2	6.3	17	11.7	3.5	39.0	3.2
			Daytime			
20x20 km^2	7.4	25.5	18.5	4.4	40.3	3.9
Plumes Model	8.3	26.9	21.2	4.9	40.4	4.3
			Nighttime			
20x20 km^2	35	360	57	21	33	12.7
Plumes Model	29.4	398	62	19	33	12.2
			Daytime Plumes Model			
Rural	7.7	8.6	7.4	2.6	37.8	2.5
Urban plumes						
0-4 hours	9.1	44.9	49.7	6.6	40.4	5.6
4-8 hours	8.1	40.2	26.9	5.4	39.8	4.7
8-12 hours	5.8	21.0	10.9	3.2	38.7	3.0
Power plant plumes						
0-4 hours	14.6	226.	*	14.2	43.8	10.7
4-8 hours	6.2	53.0	31.0	4.7	40.9	4.2
8-12 hours	4.8	19.8	11.1	2.9	38.3	2.7
			Nighttime Plumes Model			
Rural	41.0	277.	29.7	16.2	32.6	10.8
Urban plumes						
0-4 hours	4.2	406.	174.	32.4	33.0	16.3
4-8 hours	20.1	308.	123.	16.3	32.9	10.9
Power plant plumes						
0-4 hours	21.2	1300.	215.	19.0	32.9	12.0
4-8 hours	17.8	565.	57.3	13.2	32.7	9.4

The six columns give the lifetime of NO_x with respect to conversion to HNO_3, alkyl nitrates (RNO_3), peroyxacetylnitrates (PANs), all photochemical losses, dry deposition and photochemistry and dry depostion. The lifetimes are given averaged over the 20-hour simulations shown in Figure 13, and for day and night separately. Lifetimes are dependent on the temperature, wind speed, boundary layer height, etc., adopted for these particular runs.

* PAN provides a source of NO_x rather than a sink.

TABLE 5. Fate of NO_x in the Urban and Power Plant Plumes

	Urban Plume	Power Plant Plume
Conversion to HNO_3	0.48	0.56
Conversion to RNO_3	0.10	0.07
Conversion to PANs	0.17	0.15
Dry deposited	0.14	0.16
Exported to rural box	0.09	0.07

The table gives the fate of NO_x expressed as a fraction of total emissions into the plume, for plumes that were followed for 12 hours, for the simulations in Figure 13.

plume width is unrealistically low (20 km for the case shown here) the effect of the urban width on secondary species is small, less than 4%. Concentrations of NO_x are most sensitive to the urban width, increasing as width increases. Regional average concentrations are dominated by NO_x in plumes, and the NO_x lifetime increases with plume width. Regional mean and rural ozone values vary only slightly with changes in the width parameter. Peak ozone is more sensitive to urban width, since peak ozone values occur inside plumes.

The sensitivity of model results to values adopted for the width of power plant plume is somewhat less than that for the urban width (see Table 6). The effect of treating emissions in power plant plumes as continuous in the first subgrid box, rather than instantaneous, is also slight: average concentrations of ozone change by less than 1 ppbv.

The combined impact of urban and power plant emissions is included whenever emissions occur within the same NAPAP grid boxes. However, overlap between plumes from adjacent urban

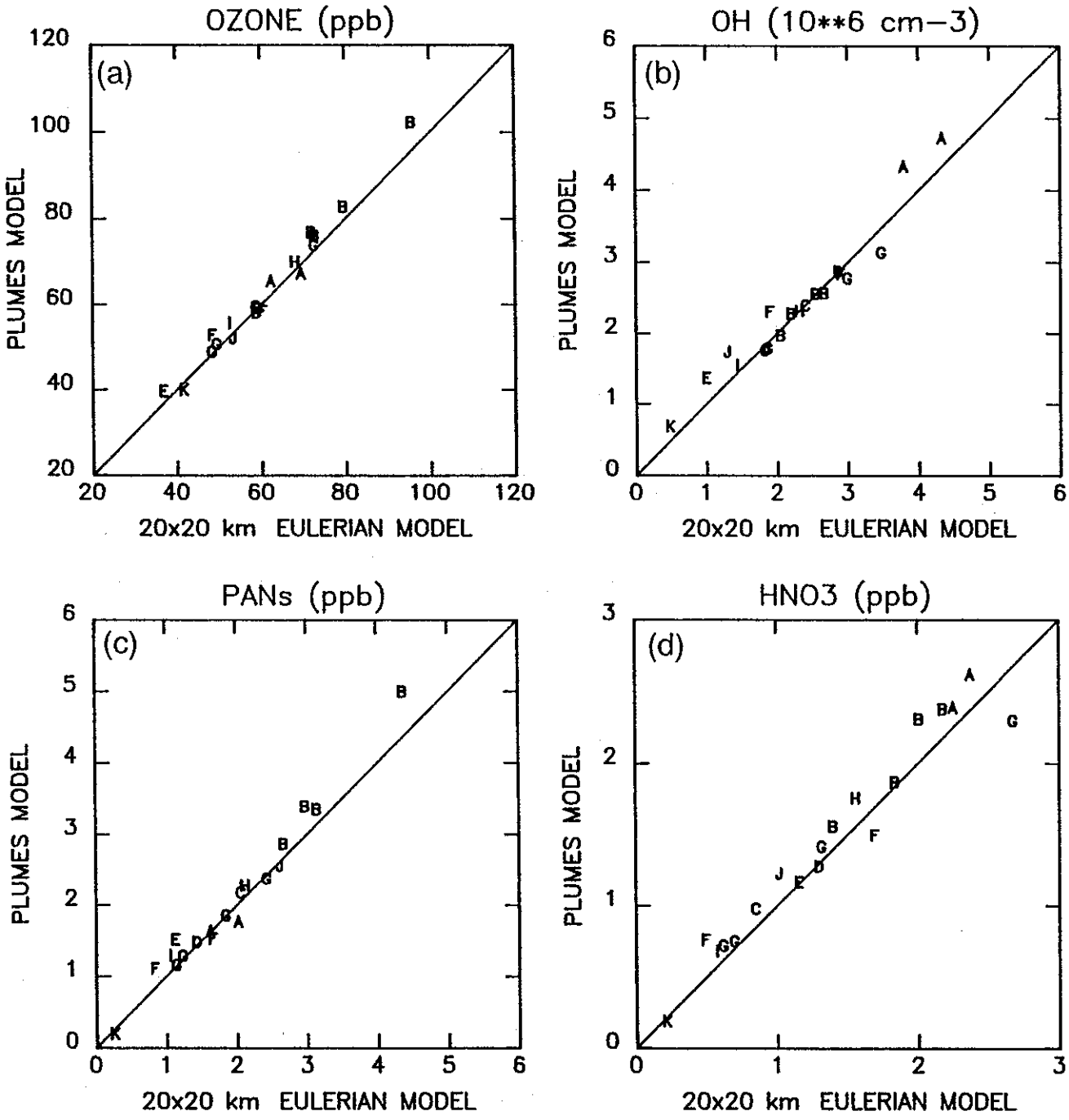

Fig. 15. Comparison of results of the Plumes model with results of the 20x20 km^2 Eulerian grid model, for the 11 test simulations described in Table 2. Results are shown for each 400x480 km^2 region, for 1600. The panels show the regional average concentration of (*a*) ozone, (*b*) OH, (*c*) PANs, (*d*) HNO_3, (*e*) NO_x, (*f*) standard deviation of NO_x, and (*g*) ozone at the ninety-eighth percentile of its cumulative distribution. Results are given in 10^6 molecules cm^{-3} for OH and parts per billion for all other species. The individual simulations are identified by the letters A-K in Table 2.

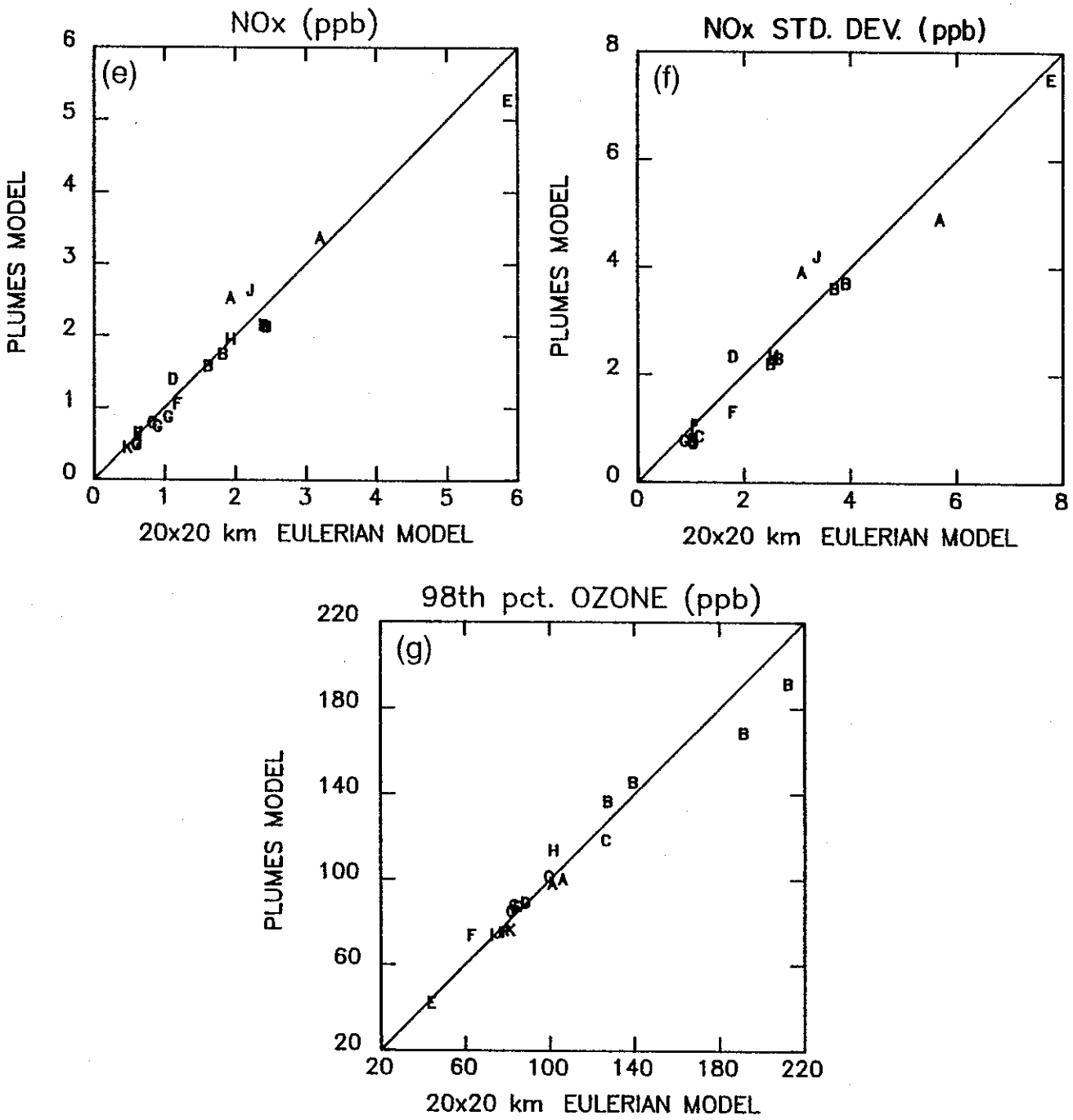

Fig. 15. (continued)

and power plant sources is not represented. We investigated the potential error introduced by ignoring possible overlap of urban and power plant plumes from adjacent sources by running the model with urban and power plant sources combined to form a single generic plume. Ozone concentrations are within ~1 ppbv of simulations with separate plumes, as shown in Table 6. Concentrations of other secondary pollutants are affected by less than 10% or less. We conclude that errors introduced by ignoring overlap between plumes from adjacent urban and power plant grid boxes are not likely to represent a major source of error.

The model does not account for interaction of aged plumes from separated urban or power plant sources during an 8-hour period after emission. Although such interactions may be locally important, for instance, when the Washington, D.C., plume passes through Baltimore, we do not expect these events to have major impact on climatological distributions or regional means. Future work is planned to investigate this question quantitatively.

8. COMPARISON OF PLUMES MODEL RESULTS WITH OBSERVATIONS

Comparison of results from the Plumes model with observations is hampered by the scarcity of representative rural data. One would like to have a network of stations making measurements continuously over a region of hundreds of kilometers in extent. It would help to have both ground-based and aircraft data. The ob-

TABLE 6. Sensitivity to Plumes Model Parameters

	O_3	NO_x	PANs	HNO_3	OH
		Urban Width y_U Varied			
y_U = 20 km	69.6	2.37	1.79	2.50	4.58
y_U = 40 km	66.3	2.68	1.67	2.49	4.47
y_U = 60 km	64.7	2.95	1.60	2.45	4.44
y_U = 80 km	64.0	3.15	1.57	2.44	4.43
		Power Plant Width y_P Varied			
y_P = 20 km	66.5	2.64	1.65	2.55	4.56
y_P = 30 km	64.8	2.93	1.61	2.44	4.39
y_P = 40 km	64.6	3.14	1.61	2.33	4.39
		Combined Plumes Width y_{PU} Varied			
y_{PU} = 40 km	66.2	3.24	1.52	2.47	4.48
y_{PU} = 60 km	63.9	3.48	1.55	2.31	4.43
y_{PU} = 80 km	62.8	3.96	1.52	2.23	4.43
Instantaneous*	65.1	2.87	1.62	2.45	4.45
Scheduled*	66.0	2.93	1.65	2.50	4.48

Average concentration of O_3, NO_x, PANs, and HNO_3 in parts per billion, and OH in 10^6 molecules cm^3 at 1600 are given for simulations with the 8-hour Plumes model with varying model assumptions.

* Power plant plumes initiated with instantaneous emissions or with scheduled emissions over 4-hour period.

servations presented by *Clarke and Ching* [1983] as part of the PEPE-NEROS study provide one of the few data sets suitable for evaluation of regional models for ozone production. Ozone concentrations were monitored on August 3-4, 1979, for a 500x500 km^2 region extending across Ohio, Pennsylvania, and New York State. A series of five airplane transects were used to measure the distribution of ozone concentrations within the region as functions of location, height, and time. The study included also a calculation of 4-day back trajectories for the air mass over the study region.

We ran a Plumes model simulation for August 1-4, 1979. According to the back trajectory calculated by Clarke and Ching, the air mass was located in Iowa and Missouri on August 1 and moved eastward through Illinois and Indiana on August 2. On August 3 and 4 the air mass moved through the regions of Ohio, western Pennsylvania, and New York State where the observations were made. The location of the air mass on these four days corresponds approximately to four adjacent grid boxes of the Plumes model, of which the center two are those shown in Figure 2. Our simulation used the two-layer vertical structure described above in section 3 with an afternoon boundary layer height of 1300 m, the value reported by Clarke and Ching. Temperature and humidity were taken from daily weather maps [*National Weather Service*, 1979]. The model was initialized at 1800, July 31, with 40 ppbv ozone, 0.25 ppbv NO_x, 200 ppbv CO, 0.08 ppbv PAN, and 12.5 ppbC nonmethane hydrocarbons. We estimated that isoprene emissions were between 1.5 and 3.0 x 10^{11} molecules $cm^{-2}s^{-1}$, based on data for isoprene fluxes and land use patterns (Lamb et al., 1987; Matthews, 1983). Anthropogenic emissions were taken from the NAPAP inventory.

The Plumes model was run in a Larangian sense for this comparison, since the observations were made following an air mass. A single 400x480 km^2 region was simulated for the 4-day period with urban, power plant, and distributed emissions based on data for the regions along the trajectory (i.e., Iowa on August 1, Illinois and Indiana on August 2, etc.). Mass fluxes were assumed to be negligible along the boundary of this region. We also ran a Plumes model Eulerian simulation for the same time period. The Eulerian simulation included the region extending from Iowa to Pennsylvania with a 5 m s^{-1} westerly wind, approximately equivalent to air mass movement along the Lagrangian trajectory. Advection between grid boxes was calculated using second-order moments [*Prather*, 1986] to account for subgrid scale gradients as described above. Predicted concentrations for locations along the air mass trajectory were derived from the Eulerian concentrations and associated moments [*Prather*, 1986].

Model results were compared with the regional average ozone concentrations and with the intraregional distribution of ozone reported by Clarke and Ching. In addition comparisons were made with observed surface ozone concentrations at individual sites that lie approximately along the air mass trajectory: Mark Twain, Missouri, on August 1, Rockport and Fort Wayne, Indiana, on August 2, Duncan Falls, Ohio, on August 3; and Scranton, Pennsylvania, on August 4. The surface stations were part of the Sulfate Regional Experiment (SURE) and the National Air Pollution Background Network (NAPBN) [*Mueller and Hidy*, 1983; *Evans et al.*, 1983; *Logan*, 1988], which ended in 1980 and 1983, respectively. There are no comparable networks in existence today.

The curves in Figure 16 show the evolution of regional average ozone concentrations in the boundary layer and in the entrainment layer for the Plumes model simulation. Lagrangian and Eulerian models agree well. The figure shows the average ozone concentrations observed during each of the five airplane transects (astericks) from the Clarke and Ching study and also observed concentrations at the five surface sites located along the air mass trajectory (crosses). The nighttime aircraft observations (arrow) should be compared with the simulated ozone concentration in the entrainment layer, because the plane operated above the nocturnal inversion. The surface stations and daytime aircraft flights sampled air in the atmospheric mixed layer. Regional ozone concentrations in the lower layer increased during the daytime because of photochemical activity and decreased at night because of deposition. Note that ozone produced during the daytime remains aloft in the upper layer at night and becomes entrained in the lower layer the following day. Ozone concentrations build up gradually throughout the 4-day simulation.

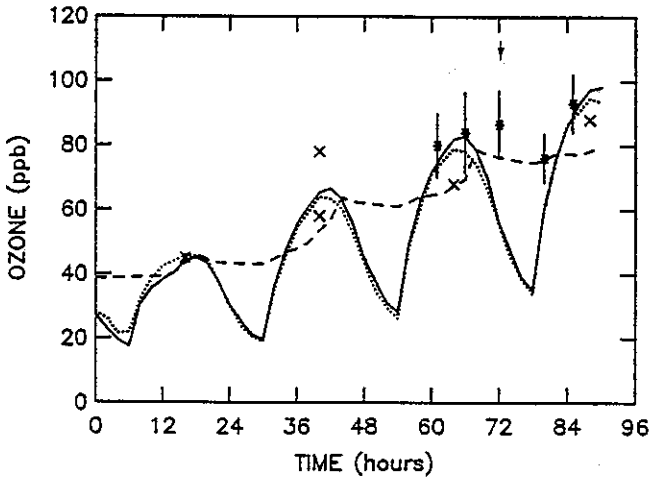

Fig. 16. Comparison of models and observations for ozone, for August 1-4, 1979. Results of the Lagrangian simulation with the Plumes model are shown by the solid line (boundary layer) and by the dashed line (entrainment layer). Results of the Eulerian simulation with the Plumes model are shown by the dotted line (boundary layer). The asterisks show the average values of ozone obtained on airplane transects, and the vertical bars give the standard deviations [*Clarke and Ching*, 1983]. Daily maximum values of ozone at surface stations are given by crosses [*Logan*, 1988]. The data are plotted at their approximate positions along the air mass trajectory. Time=0 is midnight on July 31.

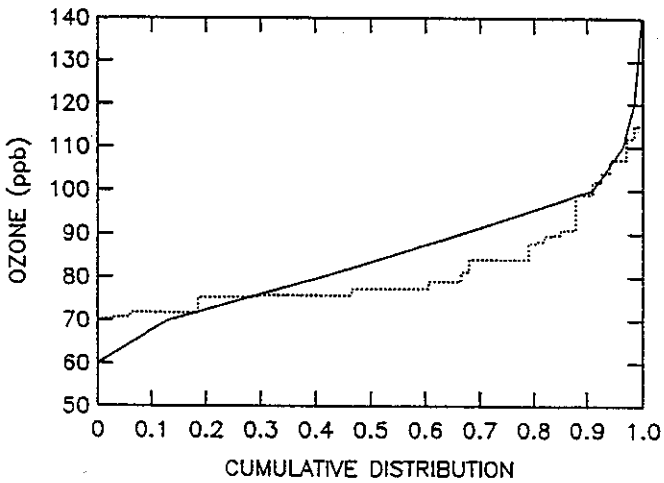

Fig. 17. Cumulative distribution of ozone, derived from five aircraft transects shown by *Clarke and Ching* [1983] for August 3-4, 1979, (solid line), compared with the distribution of ozone concentrations predicted by the Plumes model (dotted line).

Data from surface stations along the track show a buildup of daily maximum values for ozone during development of the episode. Values rose from about 45 ppbv on day 1, to 55-80 ppbv on day 2, 65 ppbv on day 3, and nearly 90 ppbv on day 4. Model results reproduce this trend well. The aircraft data show an increase of regional ozone from ~80 ppbv to ~95 ppbv during the last 2 days of the episode. Model results are similar to these observations also.

Figure 17 shows a comparison between the distribution of ozone concentrations reported by Clarke and Ching and the distribution simulated by the Plumes model. The observed distribution combines data from all five airplane transects, the model distribution likewise combines distributions from five individual times corresponding to the times of airplane transects. Model results agree with observation to within 10 ppbv, from the second to the ninety-eighth percentile of the distribution. Note that the observed ozone extremum (150 ppbv) is the result of a local thermal inversion at the eastern end of Lake Erie coinciding with the urban plume from Cleveland. The model does not include such an inversion, and this extreme value is not duplicated by the simulation.

A second opportunity for comparison of Plumes model results with observations is provided by the study of *White et al.* [1983]. They investigated the rate of export of ozone to the rural troposphere in the urban plume downwind of St. Louis and derived "ΔO_3," the difference between the rural ozone concentration and the average concentration within a plume. Their ΔO_3 can be compared directly with the difference between rural and plume concentrations in Plumes model simulations normalized by the difference between plume widths assumed in the model and widths reported by White et al.

Plumes model simulations were performed for comparison with each of the daytime observations of ΔO_3 from *White et al.* [1983]. Simulations were started 12 hours in advance of the initialization of the plume. The two-layer vertical structure was used with the time-varying mixed layer height and other meteorological parameters were adopted from observed values. Initial concentrations were the same as in the simulation described above. Simulated and observed ΔO_3 are shown in Table 7. Model results are in reasonable agreement with observation, but the model tends to underestimate ΔO_3 by a few parts per billion by volume.

TABLE 7. Comparison of Plumes Model Simulations With Urban Plume Data

Time	Wind Speed, m s^{-1}	Temperature (p.m.), °C	Boundary Layer Height, m	Obsv.[a] ΔO_3, ppb	Simulated ΔO_3, ppb	
					#1[b]	#2[c]
July 18, 1975 (12 p.m.)	9.5	29	750	29	23	21
July 18, 1975 (2 p.m.)	8.3	31	1100	23	28	22
July 18, 1975 (4 p.m.)	7.5	31	1400	22	26	28
Aug. 11, 1975 (1 p.m.)	7.0	34	1350	30	25	24
Aug. 11, 1975 (2 p.m.)	9.5	35	1350	25	25	23
July 9, 1976 (4 p.m.)	5.3	35	1150	42	40	40

[a]The difference between the average ozone concentration observed in an urban plume and the ozone concentration outside the plume reported by *White et al.* [1983], referred to in the text as ΔO_3.

[b]The difference between plume and rural ozone concentrations (ΔO_3) predicted by the Plumes model.

[c]Plumes model ΔO_3 multiplied by the ratio of model plume width to observed width [*White et al.*, 1983].

9. CONCLUSIONS

There is a need to develop models capable of simulating accurately air quality processes on regional and continental scales. To be of use to both the research and policy making communities, a regional-scale model must be capable of simulating processes for a region several thousand kilometers in extent for a period of several weeks or longer. It is important to be able to simulate the chemical climate of a region in order to elucidate the factors that influence concentrations of pollutants and the associated impact on biological systems. Existing models become prohibitively expensive in terms of the required time of computation when applied to climatological problems.

We have presented in this paper a versatile conceptual framework for regional-scale models with a broad range of potential applications. First we examined the sources of error associated with coarse resolution in Eulerian grid models. Then we developed a subgrid structure to eliminate most of this error by simulating the spatial frequency distributions for major pollutant classes. The regional model developed here is able to simulate rural atmospheric chemistry with an accuracy comparable to that of a 40x40 km^2 Eulerian grid model. The computational cost is less than a comparable fine-mesh model by a factor of 25 or more.

Our study of a regional ozone episode (section 8) demonstrates the flexibility of the methodology. The model may be either Eulerian or Lagrangian. Any number of generic plumes may be incorporated as required. Results derive from the subgrid structure and are relatively insensitive to assumed value for model parameters. A satisfactory simulation is obtained with limited computational effort.

The statistical approach adopted here merits some discussion. In order to elucidate the chemistry of atmospheric ozone on a regional scale, it is sufficient to be able to predict the statistical distribution of ozone and its precursors, fractile by fractile. We have designed a model that simulates the ensemble of observations in a regional setting, rather than attempting to simulate individual points on a fine spatial and temporal grid, the approach adopted in most models. To test the model that uses the statistical approach, we do not need data from a vast number of measurement sites, but we need to know the statistical properties of a suitable ensemble of observations including NO_x, O_3 and preferably hydrocarbons. We found one set of observations suitable for comparison; the model of subgrid plumes provided excellent capability for predicting regional mean and areal and temporal distributions of pollutant concentrations.

The present investigation is intended to lay the groundwork for a three-dimensional model of chemical climate over North America. The dynamics of this model will be provided by a global general circulation (i.e., climate) model (GCM) adapted for the purpose [*Prather et al.*, 1987; *Jacob et al.*, 1987]. The Plumes model then provides the associated ensemble of (simulated) chemical information. We anticipate that this model will be useful for the investigation of both regional and global air pollution problems. In particular we expect the model to be suitable for use in global chemical tracer experiments. We also expect the model to be useful for evaluations of proposed pollutant control strategies on the regional scale.

Acknowledgments. We wish to acknowledge the helpful comments provided by Michael McElroy, Daniel Jacob, Rose Yevich, and Jane Dignon. This work was supported by the Coordinating Research Council, Inc., (project AP-9), the National Science Foundation (ATM84-13153), and the Environmental Protection Agency (R814535-01-0).

REFERENCES

Carmichael, G. R., L. K. Peters, and T. Kitada, A second generation model for regional-scale transport/chemistry/deposition, *Atmos. Environ., 20*, 173-188, 1987.

Chang, J. S., R. A. Brost, I. S. A. Isaksen, S. Madronich, P. Middleton, W. R. Stockwell, and C. J. Walcek, A three-dimensional Eulerian acid deposition model: Physical concepts and formulation, *J. Geophys. Res., 92*, 14,681-14,700, 1987.

Ching, J. C. S., J. A. Novak, K. L. Schere, N. V. and Gilliani, Reconciling urban VOC/NO_x emission inventories with ambient concentration data, paper presented at the 80th meeting of the Air Pollution Control Association, New York, 1987.

Clarke, J. F., and J. K. S. Ching, Aircraft observations of regional transport of ozone in the northeastern United States, *Atmos. Environ., 17*, 1703-1712, 1983.

Csanady, G. T., *Turbulent Diffusion in the Environment*, D. Reidel, Hingham, Mass., 1973.

Davis, D. D., G. Smith, G. Klauber, Trace gas analysis of power plant plumes via aircraft: O_3, NO_x and SO_2 chemistry, *Science, 186*, 733-736, 1974.

DeMore, W. B., J. J. Margitan, M. J. Molina, R. T. Watson, D. M. Golden R. F. Hampson, M. J. Kurylo, C. J. Howard, and A.R. Ravishankara, Chemical kinetics and photochemical data for use in stratospheric modeling, Jet Propul. Lab., *Publ. 85-37*, Calif. Inst. Technol., Pasadena, 1985.

Environmental Protection Agency, Air quality criteria for ozone and other photochemical oxidants, *Rep. EPA/600/8-84-020-CF, EPA/600/8-84-020-EF*, Research Triangle Park, N. C., 1986*a*.

Environmental Protection Agency, Development of the 1980 NAPAP emissions inventory, *Rep. EPA/600/7-86-057a*, Research Triangle Park, N. C., 1986*b*.

Evans, G. F., P. Finkelstein, B. Martin, N. Possiel, and M. Graves, Ozone measurements from a network of remote sites, *J. Air Pollut. Control Assoc., 33*, 291-296, 1983.

Flowers, E. C., R. A. McCormick, and K. R. Kurfis, Atmospheric turbidity over the United States, 1961-1966, *J. Appl. Meteorol., 8*, 955-962, 1969.

Galbally, I. E., and C. R. Roy, Destruction of ozone at the earth's surface, *Quart. J. Roy. Meteorol. Soc., 106*, 599-620, 1980.

Garland, J. A., and S. A. Penkett, Absorbsion of PAN and O_3 by natural surfaces, *Atmos. Environ., 10*, 1127-1131, 1976.

Gifford, F. A., Horizontal diffusion in the atmosphere: A Lagrangian-dynamical theory, *Atmos. Environ., 16*, 505-512, 1982.

Guicherit, R., and H. van Dop, Photochemical production of ozone in western Europe (1971-1978) and its relation to meteorology, *Atmos. Environ., 11*, 145-155, 1977.

Heck, W. W., O. C. Taylor, R. Adams, G. Bingham, J. Miller, E. Preston, and L. Weinstein, Assessment of crop loss from ozone, *J. Air Pollut. Control Assoc., 32*, 353-361, 1982.

Hov, O., and I. S. A. Isaksen, Generation of secondary pollutants in a power plant plume: a model study, *Atmos. Environ., 15*, 2367-2376, 1981.

Hov, O., E. Hesstvedt, and I. S. A. Isaksen, Long-range transport of tropospheric ozone, *Nature, 273*, 341-344, 1978.

Huebert, B. J., Measurements of the dry deposition flux of nitric acid vapor to grasslands and forests, in *Proceedings of the 4th International Conference on Precipitation Scavenging, Dry Deposition and Resuspension*, pp. 785-794, Elevesier, New York, 1983.

Isaksen, I. S. A., O. Hov, and E. Hesstvedt, Ozone generation over rural areas, *Environ. Sci. Technol., 12*, 1279-1284. 1978*a*.

Isaksen, I. S. A., E. Hesstvedt, and O. Hov, A chemical model for urban plumes: test for ozone and particulate sulfur formation in St. Louis urban plume, *Atmos. Environ., 12*, 599-604, 1978*b*.

Jacob, D. J., and S. C. Wofsy, Photochemistry of biogenic emissions over the Amazon forest, *J. Geophys. Res., 93*, 1477-1486, 1988.

Jacob, D. J., M. J. Prather, S. C. Wofsy, and M. B. McElroy, Atmospheric distribution of ^{85}Kr simulated with a general circulation model, *J. Geophys. Res., 92*, 6614-6626, 1987.

Judeikis, H. S., and A. G. Wren, Laboratory measurements of NO and NO_2 depositions onto soil and cement surfaces, *Atmos. Environ., 12*, 2315-2319, 1978.

Lamb, B., H. Westberg, and G. Allwine, Isoprene emission fluxes determined by an atmospheric tracer technique, *Atmos. Environ., 20*, 1-8, 1986.

Lamb, B., A. Guenther, D. Gay, and H. Westberg, A national inventory of biogenic hydrocarbon emissions, *Atmos. Environ., 21*, 1695-1705, 1987.

Lamb, R. G., Numerical simulations of photochemical air pollution in the northeastern United States: ROM1 applications, *Rep. EPA-600/3-86-038*, Environ. Protection Agency, Research Triangle Park, N. C., 1986.

Liu, M. K., R. E. Morris, and J. P. Killus, Development of a regional oxidant model and application to the northeastern United States, *Atmos. Environ., 18*, 1145-1161, 1984.

Liu, S. C., M. Trainer, F. C. Fehsenfeld, D. D. Parrish, E. J. Williams, D. W. Fahey, G. Hubler, and P. C. Murphy, Ozone production in the rural troposphere and implications for regional and global ozone distributions, *J. Geophys. Res., 92*, 4191-4207, 1987.

Logan, J. A., The ozone problem in rural areas of the United States, *Proceedings of a NATO Advanced Research Workshop on Tropospheric Ozone: Regional and Global Ozone and its Environmental Consequences, NATO ASI Ser. C*, vol. 227, edited by I. S. A. Isaksen, pp. 327-344, D. Reidel, Hingham, Mass., 1988.

Logan, J. A., Ozone in rural areas of the United States, *J. Geophys. Res., 94*, 8511-8532, 1989.

Logan, J. A., M. J. Prather, S. C. Wofsy, and M. B. McElroy, Tropospheric chemistry: A global perspective, *J. Geophys. Res., 86*, 7210-7254, 1981.

Lurmann, F. W., A. C. Lloyd, and R. Atkinson, A chemical mechanism for use in long-range transport/acid deposition computer modeling, *J. Geophys. Res., 91*, 10,905-10,936, 1986.

Matthews, E., Global vegetation and land use: New high-resolution data bases for climate studies, *J. Clim. Appl. Meteorol., 22*, 474-487, 1983.

McRae, G. J., and J. H. Seinfeld, Development of a second-generation mathematical model for urban air pollution, II, Performance evaluation, *Atmos. Environ., 17*, 501-523, 1983.

Mueller, P. K., and G. M. Hidy, The Sulfate Regional Experiment (SURE): Report of findings, *Rep EA-1901*, Electric Power Res. Inst., Palo Alto, Calif., 1983.

Mukammal, E. I., H. H. Neumann, and T. R. Nichols, Some features of the ozone climatology of Ontario, Canada and possible contributions of stratospheric ozone to surface concentrations, *Arch. Meteorol. Geophys. Bioklimatol., Ser. A, 34*, 179-211, 1985.

National Weather Service, Daily weather maps, weekly series, Climate Analysis Center, NOAA, Washington, D. C., 1979.

Prather, M. J., Numerical advection by conservation of second-order moments, *J. Geophys. Res., 91*, 6671-6681, 1986.

Prather, M. J., M. B. McElroy, S. C. Wofsy, G. Russell, and D. Rind, Chemistry of the global troposphere: Fluorocarbons as tracers of air motion, *J. Geophys. Res., 92*, 6579-6613, 1987.

Schere, K. L., Modeling ozone concentrations, *Environ. Sci. Technol., 22*, 488-495, 1988.

Schere, K. L., and J. Schreffler, Final evaluation of urban-scale photochemical air quality simulation models, *Rep. EPA 600/3-82-094*, Environ. Protection Agency, 1982.

Sexton, K., and H. Westberg, Elevated ozone concentrations measured downwind of the Chicago-Gary urban complex, *J. Air Pollut. Control Assoc., 30*, 911-914, 1980.

Sillman, M. S., Models for regional scale photochemical production of ozone, Ph.D. thesis, Harvard Univ., Cambridge, Mass., 1987.

Sillman, M. S., J. A. Logan, and S. C. Wofsy, The sensitivity of ozone to nitrogen oxides and hydrocarbons in regional ozone episodes, *J. Geophys. Res., 95*, 1837-1851, 1990.

Skarby, L., and G. Sellden, The effects of ozone on crops and forests, *Ambio, 13*, 68-72, 1984.

Spicer, C. W., Nitrogen oxide reactions in the urban plume of Boston, *Science, 215*, 1095-1097, 1982.

Spicer, C. W., D. W. Joseph, P. R. Sticksel, and G. F. Ward, Ozone sources and transport in the northeastern United States, *Environ. Sci. Technol., 13*, 975-985, 1979.

Spicer, C. W., J. R. Koetz, G. W. Keigley, G. M. Sverdrup, and G. F. Ward, Nitrogen oxides reactions within urban plumes transported over the ocean, Battelle Columbus final report to the Environmental Protection Agency on contract 68-02-2957, Environ. Protection Agency, Research Triangle Park, N. C., 1981.

Trewartha, G. T., *An Introduction to Weather and Climate*, McGraw-Hill, New York, 1937.

van Ulden, A. P., and A. A. M. Holtslag, Estimation of atmospheric boundary-layer parameters for diffusion applications, *J. Clim. Appl. Meteorol., 24*, 1196-1207, 1985.

Venkatram, A., An examination of box models for air quality simulation, *Atmos. Environ., 12*, 2243-2249, 1978.

Venkatram, A., and P. Karamchandani, Source-receptor relationships: A look at acid-deposition modeling, *Environ. Sci. Technol., 20*, 1084-1091, 1987.

Wesely, M. L., J. A. Eastman, D. H. Stedman, and E. D. Yalvac, An eddy correlation measurement of NO_2 flux to vegetation and comparison to O_3 flux, *Atmos. Environ., 16*, 815-820, 1982.

Westberg, H., Ozone behavior in the combined Baltimore-Washington D.C. plume, *Rep. EPA/600/3-85/707*, Environ. Protection Agency, Research Triangle Park, N. C., 1985.

White, W. H., D. E. Patterson, and W. E. Wilson, Urban exports to the nonurban troposphere: Results for project MISTT, *J. Geophys. Res., 88*, 10,745-10,752, 1983.

Wolff, G. T., and P. J. Lioy, Development of an ozone river associated with synoptic scale episodes in the eastern United States, *Environ. Sci. Technol., 14*, 1257-1260, 1980.

J. A. Logan and S. C. Wofsy, Department of Earth and Planetary Sciences, Harvard University, Cambridge, MA 02138

S. Sillman, Department of Atmospheric, Oceanic, and Space Sciences, University of Michigan, Ann Arbor, MI 48109-2143.

(Received September 28, 1988;
revised July 12, 1989;
accepted October 5, 1989.)